Industrial Crops & Products 239 (2026) 122464

Contents lists available at ScienceDirect

Industrial Crops & Products

journal homepage: www.elsevier.com/locate/indcrop

# Steel slag - corn straw biochar composite for reducing arsenic bioavailability in paddy soil: Effectiveness and mechanisms

Xuemei Yang [a], Minling Gao [a], Weiwen Qiu [b], Youming Dong [a,*], Cheng Qiu [c,*], Zhengguo Song [a,*]

[a] Department of Materials and Environmental Engineering, Shantou University, Shantou 515063, China
[b] New Zealand Institute for Bioeconomy Science Limited, Private Bag 3230, Hamilton 3240, New Zealand
[c] Institute of Agricultural Resources and Environment, Xizang Academy of Agricultural and Animal Husbandry Sciences, Lhasa, Xizang 850032, China

ARTICLE INFO

*Keywords:*
Biochar
Steel-slag
Adsorption
Arsenic
Bioavailability

ABSTRACT

Arsenic (As) pollution poses a serious threat to both ecological systems and human health, making the development of economical and efficient remediation materials a key research priority. Steel slag (SS) and corn straw biochar (BC) are promising low-cost precursors with strong potential for As immobilization. In this study, steel slag–corn straw biochar composites (SSBCs) were produced via co-pyrolysis to elucidate their mechanisms for immobilizing As in contaminated paddy soils and inhibiting As uptake by ryegrass. Through ryegrass pot experiments and adsorption analyses, the As-reduction performance of BC, SS, and SSBCs was systematically evaluated, with particular emphasis on their effectiveness in lowering As bioavailability in paddy soil. Pot experiments revealed the application of 2 % SSBCs increased ryegrass biomass while markedly decreasing As accumulation in ryegrass roots. Furthermore, $SSBC_1$ (SS: BC= 1:1, mass ratio) and $SSBC_2$ (2.5:1) treatments elevated soil pH and significantly reduced available As concentrations. Characterization analyses indicated that the enhanced As(III) removal efficiency of $SSBC_1$ was primarily attributable to its hydroxyl, Ca–O, and Fe–O functional groups and its porous structure, which promoted surface complexation and electrostatic adsorption. In adsorption experiments, both BC and SSBCs rapidly adsorbed As(III), reaching equilibrium within 120 min. Among them, $SSBC_1$ exhibited the highest adsorption capacity (21.64 mg $g^{-1}$), representing a six-fold increase compared with BC (3.46 mg $g^{-1}$). Adsorption capacity increased under acidic conditions (pH 3.0–7.0), and $SSBC_1$ significantly enhancing soil As(III) retention. These mechanisms contributed to effective As immobilization, thereby reducing its bioavailability and subsequent plant uptake. Overall, the preparation of SSBCs improved the physicochemical properties and surface structure of BC, enhanced its adsorption performance, and demonstrated strong potential for the remediation of As-contaminated paddy soils.

## 1. Introduction

Arsenic (As) pollution is prevalent in the environment, largely due to anthropogenic activities such as mining and smelting of As and As-containing minerals, as well as the prolonged use of As-based chemicals, pesticides and herbicides (Pérez-Sirvent et al., 2016). Notably, chronic exposure to As has been associated with dermatological lesions, organ damage, cardiovascular and neurological disorders, and multiple forms of cancer (Gadd, 2009). Consequently, the International Agency for Research on Cancer (IARC) has classified arsenic in drinking water as a Group 1 human carcinogen (Luo et al., 2014). Soil As contamination is also a major concern. According to China's "National Soil Pollution Status Survey Bulletin" published in 2014, As concentrations in arable soils, such as those near realgar and coal mines (Gong et al., 2020), have exceeded permissible limits, with an exceedance rate of 2.7 %. Such contamination degrades soil functions and poses significant risks to agricultural safety. Addressing this challenge requires effective strategies to reduce the bioavailability and mobility of arsenic in soils. Among these approaches, passivation remediation has shown considerable promise, provided that efficient and economical amendment materials can be developed (Dan et al., 2023).

Steel slag (SS) is a solid by-product of iron and steel production. In 2021, China produced about 1 billion tons of crude steel, generating more than 150 million tons of SS (Liu et al., 2024; Zhang et al., 2024).

* Corresponding authors.
*E-mail addresses:* ymdong@stu.edu.cn (Y. Dong), chengqiu_2006@163.com (C. Qiu), forestman1218@163.com (Z. Song).

https://doi.org/10.1016/j.indcrop.2025.122464
Received 26 September 2025; Received in revised form 25 November 2025; Accepted 7 December 2025
Available online 11 December 2025

The growing stockpiles of SS present a significant environmental challenge, with over 70 % remaining underutilized and contributing to farmland disruption, water contamination, and air pollution (Dippenaar, 2005; Guo et al., 2018). Notably, SS contains components such as CaO, $SiO_2$, and FeO, and exhibits inherent alkalinity and adsorption capacity when processed into fine particles (Kim et al., 2021). These properties enable SS to immobilize As through precipitation, adsorption, and co-precipitation mechanisms (Li, Qi, et al., 2021; Shi et al., 2018). However, despite its potential for As detoxification, the practical use of SS remains constrained by factors such as low removal efficiency, limited adsorption capacity, and the risk of excessively increasing soil pH. To address these limitations, recent studies have explored combining SS with biomass-derived materials, which significantly improves the composite's physical properties and ultimately enhances its potential for soil remediation (Tian et al., 2025).

Among these biomass-derived materials, biochar produced through the thermal pyrolysis of agricultural residues such as corn straw has a porous structure and a large specific surface area, giving it a measurable capacity to adsorb As (Lehmann and Joseph, 2009). However, the intrinsic adsorption capacity of biochar for As is limited. In practical applications, biochar often requires modification to improve its adsorption performance (Jin et al., 2014). For example, Khan et al. (2020) reported that molybdenum disulfide-impregnated $FeO_x$@BC800, prepared via the hydrothermal method, achieved effective As(III) removal from aqueous solutions. Similarly, nano zero-valent iron--modified biochar has been shown to reduce As bioavailability in soils, lowering As accumulation in vegetables by 21.99–35.01 % (Yang et al., 2021). Nevertheless, the high cost of many modification reagents limits their suitability for large-scale applications. In this context, using low-cost, Fe-rich steel slag as a modifier for biochar offers a promising "waste-treating-waste" strategy. Although some studies have reported synergistic effects between SS and biochar in alleviating heavy metal stress in plants (Kapoor and Hasanuzzaman, 2024), systematic investigations into the mechanisms of steel slag–modified biochar composites in arsenic-contaminated soils remain scarce. Therefore, this study aims to synthesize a novel composite material using steel slag and corn straw biochar and to evaluate its effectiveness and underlying mechanisms in reducing As bioavailability in soil. Through a combination of pot experiments, adsorption tests, and material characterization analyses, we seek to elucidate the immobilization behavior and interactions between the composite and arsenic, thereby providing a scientific foundation for developing cost-effective remediation strategies for As-contaminated soils.

## 2. Materials and methods

### 2.1. Materials

Corn straw, an agricultural waste material, was collected from the farmland in Tianjin, China, referring specifically to the above-ground residues remaining after corn ear harvest. Steel slag powder (SS) was obtained from Tangshan Iron and Steel Group Co., Ltd. (Tangshan, Hebei Province, China), with a median particle size was 13.2 μm, measured using a Malvern Mastersizer (Malvern Instruments Ltd., UK). An As(III) solution ($Na_2AsO_3$, 1000 mg $L^{-1}$) was purchased from Inorganic Ventures Co. (Virginia, USA), and all other analytical-grade chemicals were supplied by Xilong Science Co., LTD (Shantou, Guangdong Province, China). All experiments were conducted using deionized water with a resistivity of 18.25 MΩcm$^{-1}$.

### 2.2. Biochar preparation

Corn straw biochar (BC): Collected corn straw was oven-dried at 60 °C, ground, passed through a 100-mesh nylon sieve, weighed, and placed in a crucible. The samples were then subjected to pyrolysis in a tube furnace. Nitrogen gas was purged for 20 min at a flow rate of 6000 $cm^3 \cdot min^{-1}$ to create an oxygen-free environment. During pyrolysis, nitrogen continued to flow while the samples were heated at 10 °C·min$^{-1}$ to 600 °C and maintained for 2 h (Lin et al., 2019), producing BC.

Steel slag-corn straw biochar composites (SSBCs): SS and BC were mixed at mass ratios of 1:1, 2.5:1, and 10:1, designated as $SSBC_1$, $SSBC_2$, and $SSBC_3$, respectively. To prepare the composites, predetermined amounts of BC and SS were placed into a crucible, followed by the addition of 40 mL of deionized water. The mixture was stirred thoroughly and evaporated in a 95 °C water bath (Lian et al., 2020). After drying, the mixtures were co-pyrolyzed under the same conditions used for BC preparation (600 °C for 2 h under an $N_2$ atmosphere), based on previous experiments and literature methods (Lin et al., 2019). The physicochemical properties, scanning electron micrographs (SEM), Fourier transform infrared (FTIR) spectra, and X-ray photoelectron spectroscopy (XPS) results of SS, BC, and SSBCs are presented in the Supporting Information (SI).

### 2.3. Pot experiment

#### 2.3.1. Ryegrass seeds

Ryegrass (Lolium perenne L) seeds were purchased from Jiangsu Chuhan Seed Industry Co., Ltd. (Suqian, Jiangsu Province, China). Seeds of uniform size were surface-sterilized with 5 % sodium hypochlorite solution for 15 min and rinsed several times with deionized water. The seeds were then germinated in 9 mm petri dishes at 25 °C in a constant-temperature incubator (POX 330A-12HM, Ningbo Life Technology Co., Ltd., Zhejiang, China) in the dark form May 30th to June 4th, after which they were transferred to an artificial climate chamber at Shantou University (Shantou, Guangdong Province, China) with controlled conditions of 25 °C temperature, 70 % relative humidity, and 12 h $d^{-1}$illumination.

#### 2.3.2. Pot experiment

Two types of As-contaminated paddy soils (classified as Ultisols, USDA system), one with high and one with low arsenic levels, were collected from the plow layer (0–20 cm) in Foshan City, Guangdong Province. Soil samples were air-dried, finely ground, and sieved through 3 mm nylon mesh. The key physicochemical properties of the soils were as follows for the low- and high-As soils, respectively: pH, 7.02 and 6.13; organic matter, 26.30 and 16.65 g $kg^{-1}$ ; total As, 71.81 and 109.77 mg $kg^{-1}$ ; and available As, 0.35 and 0.84 mg $kg^{-1}$ . Their physicochemical properties are shown in Table 2 (Supporting Information).

For the pot trial, 1.5 kg of each soil was weighed into pots. Each pot measured 16 cm in height, 15.5 cm in top diameter and 13.5 cm bottom diameter. A total of 96 pots were used. For soil amendment, five materials (SS, BC, $SSBC_1$, $SSBC_2$, $SSBC_3$) were applied at rates of 0.5 % (7.5 g $pot^{-1}$), 1 % (15 g $pot^{-1}$), and 2 % (30 g $pot^{-1}$) of soil weight. Each contaminated soil type received 16 treatments, including a control (no amendment) and soil treated with the five materials at the three aforementioned rates. All treatments were triplicated and randomly arranged. Before transplanting, treated soils were saturated with deionized water and equilibrated for 2 weeks. Fertilizers were applied at N 0.2 g·$kg^{-1}$ , P 0.1 g·$kg^{-1}$ , and K 0.2 g·$kg^{-1}$ . After two weeks, 25 germinated ryegrass seedlings were transplanted per pot. Each pot received 100 mL deionized water every two days to maintain consistent moisture. Ryegrass growth lasted for a total of 60 days from June 4th to August 5th in a controlled-climate chamber.

#### 2.3.3. As content in ryegrass

Harvested plants were washed with deionized water and separated into roots and shoots. Samples were oven-dried at 80 °C and stored at 25 °C until analysis. Dried tissues (0.2 g) were digested in $HNO_3$ using a graphite digestion system (LabTech Inc., Hopkinton, MA, USA) at 135 °C for 2 h (Chen et al., 2023; Liu et al., 2015). After cooling, the digests were filtered through Whatman No. 42 paper. Arsenic concentrations

were determined by atomic fluorescence spectrometry (AFS-9760, Beijing Haiguang Instrument Co., Beijing, China). Mixed standards were run with every 10 samples. Recovery ranged from 94.6 %–101.0 %, with relative standard deviations < 3.1 %.

#### 2.3.4. Soil properties and available As

Soil samples collected from the pots were air-dried, ground, and passed through a 2 mm sieve for subsequent analyses.

Soil pH was measured as follows: A 10 g subsample of soil was mixed with 25 mL of ultrapure water, stirred thoroughly, and allowed to stand for 30 min. The pH of the supernatant was determined using a calibrated pH meter (Yamada et al., 2010). Active organic matter was determined using the $KMnO_4$ oxidation method (LEFROY et al., 1993; Loginow et al., 1987): Soil was mixed with 25 mL of 333 mmol·$L^{-1}$ $KMnO_4$ solution in a centrifuge tube, shaken at 150 rpm for 1 h, and centrifuged at 2000 rpm for 5 min. The supernatant was diluted 1:250 with ultrapure water, and absorbance was measured at 565 nm. Active carbon content was calculated assuming that 1 mmol·$L^{-1}$ $KMnO_4$ oxidizes 9 mg of carbon. Available As was determined following Yuan et al. (2007): A 0.2 g portion of soil was extracted three times with a mixed solution of 1 mol·$L^{-1}$ $H_3PO_4$ and 0.1 mol·$L^{-1}$ ascorbic acid at 98 °C for 3 h. The extracts were combined, adjusted to a final volume of 50 mL, and the arsenic concentration was quantified by atomic fluorescence spectrometry (AFS-9760).

#### 2.3.5. Soil enzyme activity

Enzyme activities, including soil catalase (S-CAT), peroxidase (S-POD), alkaline phosphatase (S-AKP), and urease (S-UE), were measured as follow:

S-CAT was measured based on the decrease in absorbance at 240 nm after the reaction of $H_2O_2$ with catalase (Jin et al., 2009). S-POD was determined by quantifying quinone formation at 430 nm resulting from the oxidation of organic matter (Hunting et al., 1959). S-AKP was measured by treating soil with disodium phenyl phosphate and quantifying phenol formation at 660 nm (Boyd and Mortland, 2017). S-UE was determined by incubating 0.05 g soil with uric acid at 37 °C for 24 h, with released $NH_3$ quantified at 578 nm (Kandeler and Gerber, 1988).

### 2.4. Adsorption experiment

#### 2.4.1. Adsorption kinetics

Kinetic studies were performed by adding 0.25 g of sample to 250 mL of 50 mg·$L^{-1}$ As(III) solution, shaken at 25 °C and 180 rpm. Aliquots (1 mL) were collected at 0–1440 min intervals, filtered through 0.22 μm membranes, diluted, and analyzed for As concentration using AFS-9760.

#### 2.4.2. Adsorption isotherms

Composite (0.02 g) was added to 40 mL glass bottles containing 20 mL As(III) solutions (2.5–50 mg·$L^{-1}$). Bottles were shaken at 25 °C and 180 rpm for 24 h in triplicate. After filtration (0.22 μm), As concentrations were determined by an AFS-9760.

#### 2.4.3. Effect of pH on the adsorption

Composite (0.02 g) was added to 20 mL As(III) solutions at pH 3–7, adjusted with 0.1 mol·$L^{-1}$ NaOH/$HNO_3$. Adsorption was evaluated as described for isotherms.

#### 2.4.4. Soil adsorption

Soil (2 g) was amended with 0, 0.5 %, 1 %, and 2 % SS, BC, or $SSBC_1$ and equilibrated with 20 mL As(III) solutions of varying concentrations. Adsorption experiments were repeated as described above.

### 2.5. Characterization methods

An elemental analyzer (EA; Elementar VARIOEL cube, Germany) was used to determine the carbon, hydrogen, nitrogen and sulphur contents of the adsorbent. The surface area and pore structure of the samples were analyzed using a NOVA 1200e surface area and pore analyzer (BELSORP-max, Japan), and the specific surface area was calculated based on the Brunauer–Emmett–Teller (BET) isotherm obtained from nitrogen adsorption–desorption measurements. Scanning electron microscopy (SEM; ZEISS GeminiSEM 500, Germany) was employed to examine the surface morphology of the materials. Elemental composition was analyzed by X-ray photoelectron spectroscopy (XPS; Thermo Scientific ESCALAB 250, USA). Functional groups were identified by Fourier transform infrared spectroscopy (FTIR; Nicolet iS5, Thermo Fisher Scientific, USA) over 400–4000 $cm^{-1}$ .

### 2.6. Data analysis

All treatments were performed with triplicates. Data were preprocessed using Microsoft Excel 2021 (Microsoft Co., Washington, USA), and were presented as mean ± standard deviation. Statistical analyses were performed using the SPSS 17.0 software (SPSS Inc., Chicago, USA). Prior to analysis, the assumptions of normality (Shapiro–Wilk test) and homogeneity of variances (Levene's test) were assessed, and the data were confirmed to meet both requirements. Analysis of variance (ANOVA) was applied to test the significance of the treatment effects, followed by one-way ANOVA and Duncan's multiple range tests at the 0.05 significance level ($p < 0.05$). Statistically significant differences between treatment means are indicated with different lowercase letters in the figures and tables. Curve fitting and graph plotting were performed using Origin 2021 (OriginLab Co., Northampton, USA).

## 3. Results

### 3.1. Effects of composite materials on ryegrass growth

Ryegrass growth responded significantly to the amendment treatments, with higher application rates generally leading to increased biomass production ($p < 0.05$; Table 1). In general, higher amendment rates produced greater changes in biomass. In the low-As soil, total biomass increased significantly relative to the control under the following treatments: 2 % SS, 1 % $SSBC_1$, 2 % $SSBC_1$, 1 % $SSBC_2$, 2 % $SSBC_2$ and 2 % $SSBC_3$ treatments. In the high-As soil, significant biomass increases were observed with 1 % $SSBC_1$, 2 % $SSBC_1$ and 2 % $SSBC_2$. Notably, $SSBC_1$ consistently enhanced both root and shoot biomass in both soil types, increasing total biomass by 7.80 g in low-As soil and 5.71 g in high-As soil compared with the control. This demonstrates its strong ability to mitigate As toxicity and promote ryegrass growth.

### 3.2. As content of ryegrass

As concentrations in ryegrass were significantly affected by the soil amendments ($p < 0.05$) (Table 2). As expected, roots accumulated more As than shoots, consistent with root-to-shoot transport. Relative to the control, all amendments reduced As in both roots and shoots, and the removal rate generally increased with application rate. In the low-As soil, adding 2 % SS, BC, $SSBC_1$, $SSBC_2$, and $SSBC_3$ reduced root As by 51.80 %, 51.63 %, 78.89 %, 60.10 %, and 57.30 %, respectively; corresponding shoot reductions were 70.07 %, 62.05 %, 73.20 %, 73.05 %, and 61.69 %. Similar trends were observed in the high-As soil, where $SSBC_1$ again showed the highest reduction in both tissues, underscoring its efficacy in limiting As uptake and translocation.

### 3.3. Effects of composite materials on soil pH

To assess amendment effects on soil acidity/alkalinity, soil pH was measured after harvest in both contamination levels. As shown in Fig. 1 (a), all treatments significantly increased pH relative to the control, with greater increases at higher application rates ($p < 0.05$). In the low-As soil, 2 % SS, 2 % $SSBC_1$ and 2 % $SSBC_3$ treatments increased pH by

**Table 1**
Biomass of ryegrass under different treatments (g pot$^{-1}$).

| Treatments | Low As-contaminated soil | | | High As-contaminated soil | | |
|---|---|---|---|---|---|---|
| | Root | Shoot | Total biomass | Root | Shoot | Total biomass |
| CK | 0.58 ± 0.052e | 1.47 ± 0.122d | 2.05 ± 0.070e | 0.54 ± 0.058e | 1.30 ± 0.114 f | 1.84 ± 0.160e |
| 0.5 % SS | 0.65 ± 0.020e | 2.02 ± 0.081d | 2.67 ± 0.099e | 1.06 ± 0.081bcde | 2.00 ± 0.099ef | 3.06 ± 0.179de |
| 1.0 % SS | 1.67 ± 0.034abc | 2.55 ± 0.207 cd | 4.21 ± 0.380cde | 1.42 ± 0.200cde | 2.44 ± 0.023ef | 3.86 ± 0.250de |
| 2.0 % SS | 2.04 ± 0.098de | 3.84 ± 0.95ab | 5.88 ± 0.852ab | 2.11 ± 0.092a | 3.64 ± 0.543bc | 5.75 ± 0.852b |
| 0.5 % BC | 0.70 ± 0.002e | 2.06 ± 0.047d | 2.76 ± 0.045e | 1.04 ± 0.046e | 2.03 ± 0.014 f | 3.28 ± 0.060e |
| 1.0 % BC | 0.76 ± 0.012e | 2.61 ± 0.047d | 3.37 ± 0.06de | 1.54 ± 0.165bcd | 2.55 ± 0.129def | 3.97 ± 0.32cde |
| 2.0 % BC | 1.17 ± 0.084 cd | 3.67 ± 0.623abc | 4.84 ± 0.818bcd | 1.79 ± 0.047bc | 3.54 ± 0.166cde | 5.33 ± 0.015bcd |
| 0.5 % $SSBC_1$ | 0.90 ± 0.041de | 2.78 ± 0.352 cd | 3.68 ± 0.384cde | 1.16 ± 0.006de | 2.71 ± 0.071ef | 3.87 ± 0.065cde |
| 1.0 % $SSBC_1$ | 1.40 ± 0.087ab | 4.32 ± 0.542abc | 5.72 ± 1.124ab | 2.10 ± 0.381a | 4.16 ± 0.344a | 6.27 ± 0.725ab |
| 2.0 % $SSBC_1$ | 2.68 ± 0.232a | 7.17 ± 0.503a | 9.85 ± 0.735a | 2.61 ± 0.006a | 4.95 ± 0.054a | 7.55 ± 0.060a |
| 0.5 % $SSBC_2$ | 0.97 ± 0.168de | 2.23 ± 0.488bcd | 3.20 ± 0.622cde | 0.86 ± 0.023e | 1.88 ± 0.007 f | 2.74 ± 0.030e |
| 1.0 % $SSBC_2$ | 1.37 ± 0.161ab | 3.91 ± 0.106a | 6.38 ± 0.230ab | 1.31 ± 0.087de | 2.84 ± 0.237 f | 4.15 ± 0.375 cd |
| 2.0 % $SSBC_2$ | 2.47 ± 0.126ab | 5.72 ± 0.628a | 7.09 ± 0.731ab | 1.89 ± 0.184b | 4.03 ± 0.681ab | 5.92 ± 0.865be |
| 0.5 % $SSBC_3$ | 1.19 ± 0.087de | 3.21 ± 0.416 cd | 4.65 ± 0.496cde | 0.66 ± 0.080e | 2.14 ± 0.049 f | 2.80 ± 0.221e |
| 1.0 % $SSBC_3$ | 1.44 ± 0.111e | 4.33 ± 0.232 cd | 5.52 ± 0.342cde | 1.06 ± 0.065e | 3.50 ± 0.066ef | 4.56 ± 0.18 cd |
| 2.0 % $SSBC_3$ | 1.89 ± 0.244ab | 5.42 ± 0.530abc | 7.31 ± 0.785abc | 1.95 ± 0.014de | 4.43 ± 0.175cdef | 6.38 ± 0.282ab |

Note: SS is steel slag; BC is corn straw biochar; SS and BC were mixed at mass ratios of 1:1, 2.5:1, and 10:1, labeled $SSBC_1$, $SSBC_2$, and $SSBC_3$; different letters indicate significant differences at $p < 0.05$; the same letter indicates no significant difference.

**Table 2**
As concentrations in ryegrass tissues under different treatments (mg kg$^{-1}$) and reduction rates (%).

| Treatments | Low As-contaminated soil | | | | High As-contaminated soil | | | |
|---|---|---|---|---|---|---|---|---|
| | Root | Reduction rate | Shoot | Reduction rate | Root | Reduction rate | Shoot | Reduction rat |
| CK | 89.34 ± 0.12ab | — | 13.73 ± 0.38a | — | 163.77 ± 10.22a | – | 7.04 ± 0.33a | — |
| 0.5 % SS | 87.75 ± 10.21ab | 1.78 | 12.96 ± 2.22a | 5.61 | 110.92 ± 18.80ab | 32.27 | 6.20 ± 3.55ab | 11.93 |
| 1.0 % SS | 85.83 ± 4.26ab | 3.93 | 4.86 ± 0.32 cd | 64.60 | 98.92 ± 25.41abc | 39.60 | 5.54 ± 1.98ab | 21.31 |
| 2.0 % SS | 43.06 ± 3.58 cd | 51.80 | 4.11 ± 0.21d | 70.07 | 70.74 ± 13.53bc | 56.81 | 4.64 ± 1.71ab | 34.09 |
| 0.5 % BC | 76.64 ± 28.22abc | 14.22 | 6.89 ± 1.72bcd | 49.82 | 112.93 ± 45.01ab | 31.04 | 5.81 ± 0.10ab | 17.47 |
| 1.0 % BC | 74.13 ± 9.12abc | 17.02 | 5.99 ± 1.62 cd | 57.37 | 59.00 ± 33.71bc | 63.97 | 5.02 ± 2.37ab | 28.69 |
| 2.0 % BC | 43.21 ± 2.43 cd | 51.63 | 5.21 ± 0.82 cd | 62.05 | 56.80 ± 12.38bc | 65.32 | 4.52 ± 1.56b | 35.80 |
| 0.5 % $SSBC_1$ | 59.40 ± 9.66 cd | 33.51 | 4.30 ± 0.45 cd | 68.68 | 91.78 ± 55.52bc | 43.96 | 5.28 ± 1.63ab | 25.00 |
| 1.0 % $SSBC_1$ | 44.06 ± 12.16 cd | 50.68 | 4.07 ± 0.26d | 70.36 | 61.94 ± 18.18bc | 62.18 | 5.19 ± 0.40ab | 26.28 |
| 2.0 % $SSBC_1$ | 18.86 ± 5.57d | 78.89 | 3.68 ± 0.94d | 73.20 | 30.20 ± 3.70c | 81.56 | 4.13 ± 1.44b | 41.34 |
| 0.5 % $SSBC_2$ | 44.90 ± 5.67 cd | 49.74 | 4.81 ± 0.54d | 64.97 | 79.59 ± 5.24bc | 51.40 | 6.64 ± 0.93ab | 5.68 |
| 1.0 % $SSBC_2$ | 39.44 ± 3.01 cd | 55.85 | 4.09 ± 0.70d | 70.36 | 54.78 ± 8.08bc | 66.55 | 5.54 ± 2.48ab | 21.31 |
| 2.0 % $SSBC_2$ | 35.65 ± 6.90 cd | 60.10 | 3.70 ± 0.78d | 73.05 | 52.97 ± 21.45bc | 67.66 | 5.49 ± 2.84ab | 22.02 |
| 0.5 % $SSBC_3$ | 60.14 ± 37.83bcd | 32.68 | 9.28 ± 1.18d | 32.41 | 107.33 ± 1.36ab | 34.46 | 6.80 ± 0.35ab | 3.41 |
| 1.0 % $SSBC_3$ | 51.56 ± 19.87bcd | 42.29 | 8.33 ± 0.17bc | 39.33 | 99.99 ± 0.76abc | 38.94 | 5.99 ± 0.39ab | 14.91 |
| 2.0 % $SSBC_3$ | 38.15 ± 2.72 cd | 57.30 | 5.26 ± 1.16 cd | 61.69 | 55.45 ± 6.13bc | 66.14 | 5.12 ± 0.38ab | 27.27 |

Note: SS is steel slag; BC is corn straw biochar; SS and BC were mixed at mass ratios of 1:1, 2.5:1, and 10:1, labeled $SSBC_1$, $SSBC_2$, and $SSBC_3$; different letters indicate significant differences at $p < 0.05$; the same letter indicates no significant difference.

15.47 %, 6.33 % and 9.89 %, respectively. In the high-As soil, the most pronounced increases were observed with 2 % SS and 2 % $SSBC_1$ (15.46 % and 13.15 %), suggesting a consistent alkalizing effect of the composites.

### 3.4. Effects of composite materials on active organic matter

Active ($KMnO_4$-oxidizable) organic matter content increased across all treatments, following the order: $SSBC_1 > SSBC_2 > SSBC_3 > BC > SS$ (Fig. 1b). In the low-As soil, 2 % $SSBC_1$, 2 % $SSBC_2$, and 2 % $SSBC_3$ increased active organic matter by 22.37 %, 18.22 %, and 17.04 %, respectively, compared with the control. The corresponding increases in the high-As soil were even greater (32.03 %, 30.61 %, 29.27 %). Although active organic matter tended to rise with increasing application rate, these trends were not statistically significant ($p > 0.05$).

### 3.5. Effects of composite materials on the available As

As shown in Fig. 1(c), the application of SSBCs significantly affected the concentration of available As in soil ($p < 0.05$). In particular, $SSBC_1$ reduced available As by 37.87 %–55.51 % in the low-As soil and by 18.91 %–28.38 % in the high-As soil. However, compared with treatments using SS or BC alone, the application of SSBCs did not result in a statistically significant difference in available As concentrations ($p > 0.05$).

### 3.6. Effects of composite materials on soil enzyme activity

Soil enzyme activities showed variable responses to the amendments, reflecting differences in both soil As levels and the compositions of the applied materials. As shown in Fig. 2(a), S-CAT activity increased following the application of both raw and composite materials, with a clear upward trend as application rates increased. Compared with the control, S-CAT activity increased by 16.68 % in the low-As soil and by 112.86 % in the high-As soil after the addition of 2 % $SSBC_1$. These results suggest that SSBCs enhance microbial abundance and activity, while also contributing to increases in soil organic matter content. Notably, SSBCs showed a stronger capacity to promote S-CAT activity in high-As soil.

In contrast, S-POD activity displayed an opposite trend relative to the other enzymes (Fig. 2b). POD activity in untreated high-As soil was 1.9 times higher than in low-As soil. The application of amendments had contrasting effects: S-POD activity was stimulated in low-As soil but suppressed in high-As soil. For example, $SSBC_1$ increased S-POD activity

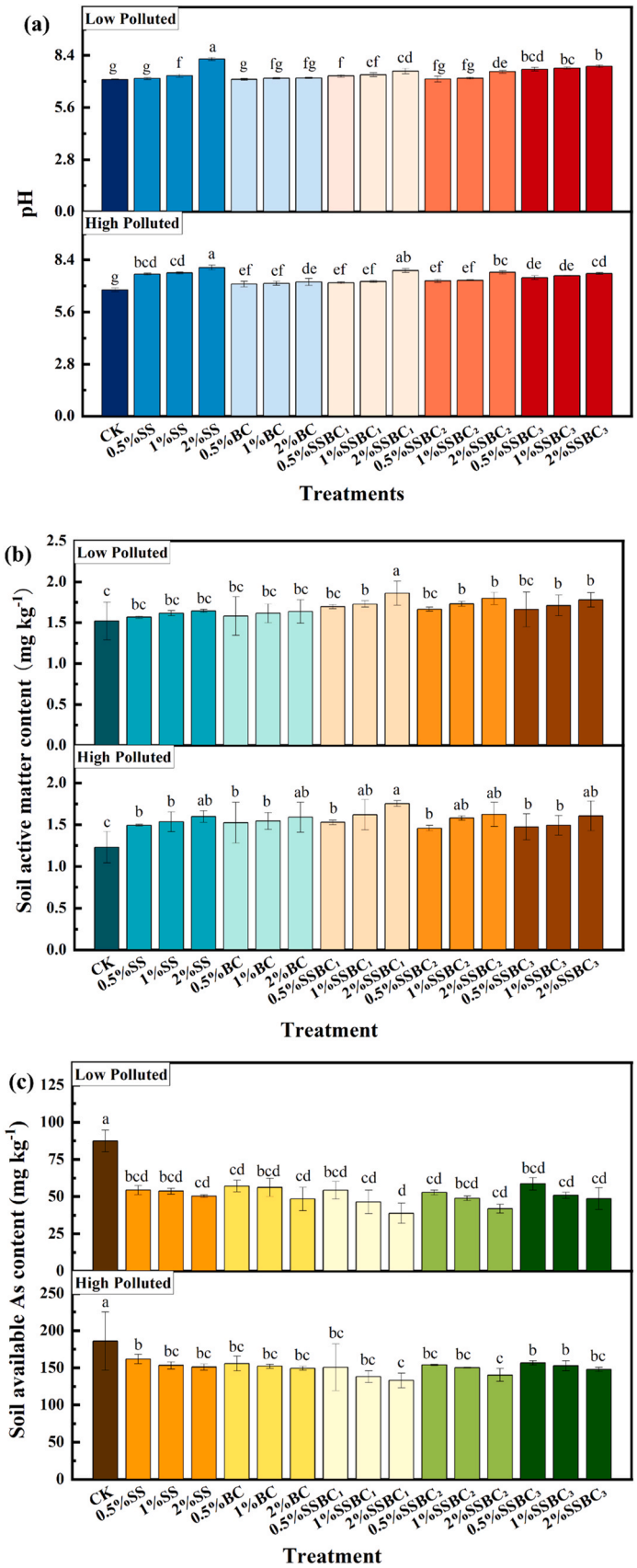


**Fig. 1.** Soil properties and available As under different treatment: (a) Soil pH; (b) Soil active organic matter content; (c) Soil available As content. (SS = steel slag; BC= corn straw biochar; SS and BC were mixed at mass ratios of 1:1, 2.5:1, and 10:1, labeled $SSBC_1$, $SSBC_2$, and $SSBC_3$; Different colors represent different materials; different letters indicate significant differences at $p < 0.05$; the same letter indicates no significant difference).

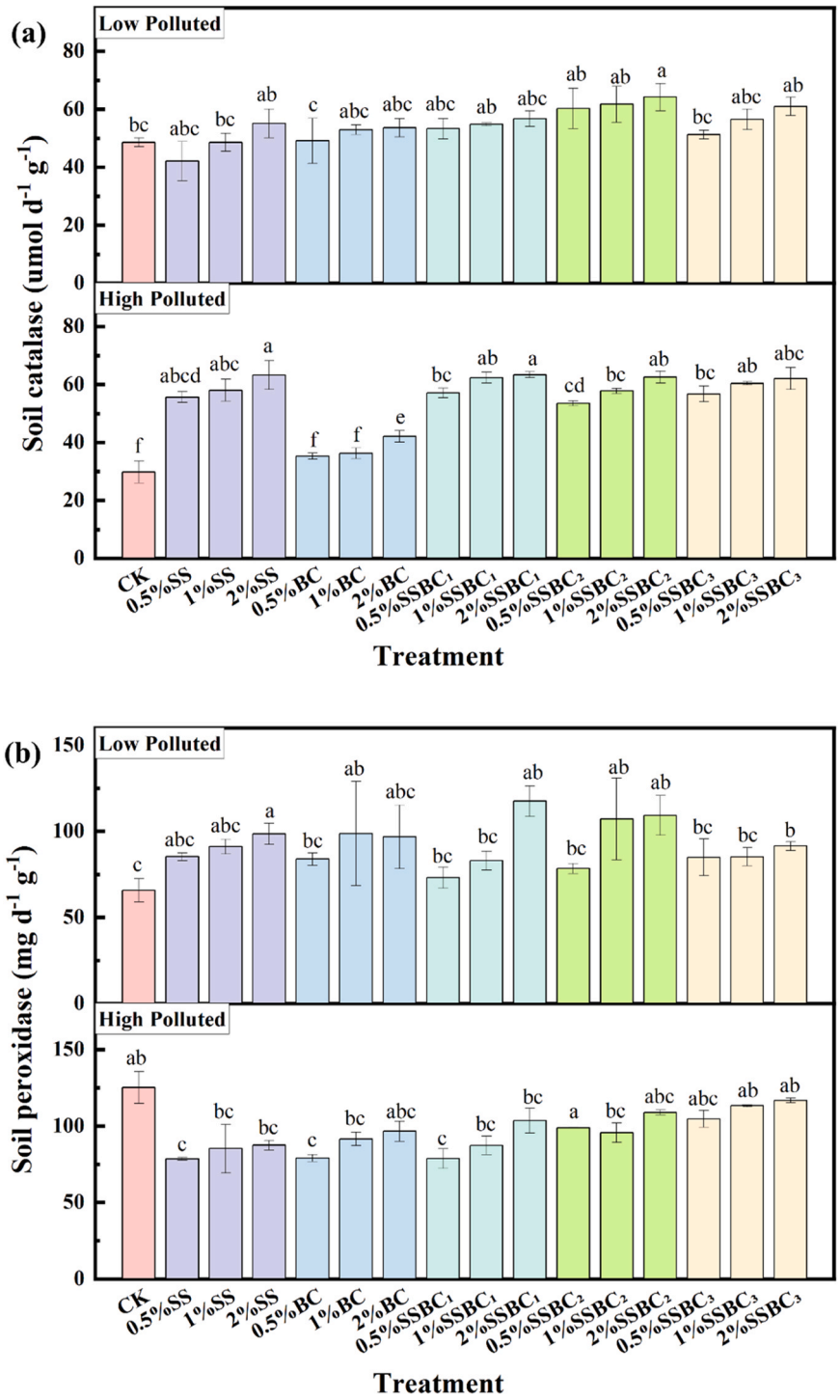


**Fig. 2.** Effects of SSBCs supplementation on soil enzyme activity in ryegrass soil:(a) S-CAT (soil catalase); (b) S-POD (soil peroxidase); (c) S-AKP (soil alkaline phosphatase); (d) S-UE (soil urease). (SS = steel slag; BC = corn straw biochar; SS and BC were mixed at mass ratios of 1:1, 2.5:1, and 10:1, labeled $SSBC_1$, $SSBC_2$, and $SSBC_3$. Different colors represent different materials. different letters indicate significant differences at $p < 0.05$; the same letter indicates no significant difference).

in low-As soil by 11.12 %–78.73 %, whereas it decreased activity in high-As soil by 17.30–37.15 %.

As shown in Fig. 2(c), untreated low-As soil exhibited 2.93 times higher S-AKP activity than untreated high-As soil. In low-As soil, both raw and composite amendments significantly inhibited S-AKP activity ($p < 0.05$). Compared with the control, $SSBC_1$ reduced S-AKP activity in low-As soil by 26.04 %–55.45 %. In high-As soil, SS and BC generally suppressed S-AKP activity, whereas low application rates of the composites promoted it. Specifically, 0.5 % $SSBC_1$, 1 % $SSBC_1$, 0.5 % $SSBC_2$, and 0.5 % $SSBC_3$ increased S-AKP activity by 18.46 %, 42.99 %, 11.04 %, and 2.91 %, respectively, compared with the control.

Finally, changes in S-UE activity (Fig. 2d) were broadly consistent with those observed for S-AKP. Untreated low-As soil showed 3.26 times higher S-UE activity than untreated high-As soil. Relative to the control, all amendments significantly enhanced S-UE activity in high-As soil ($p < 0.05$). In low-As soil, BC treatment increased S-UE activity, whereas

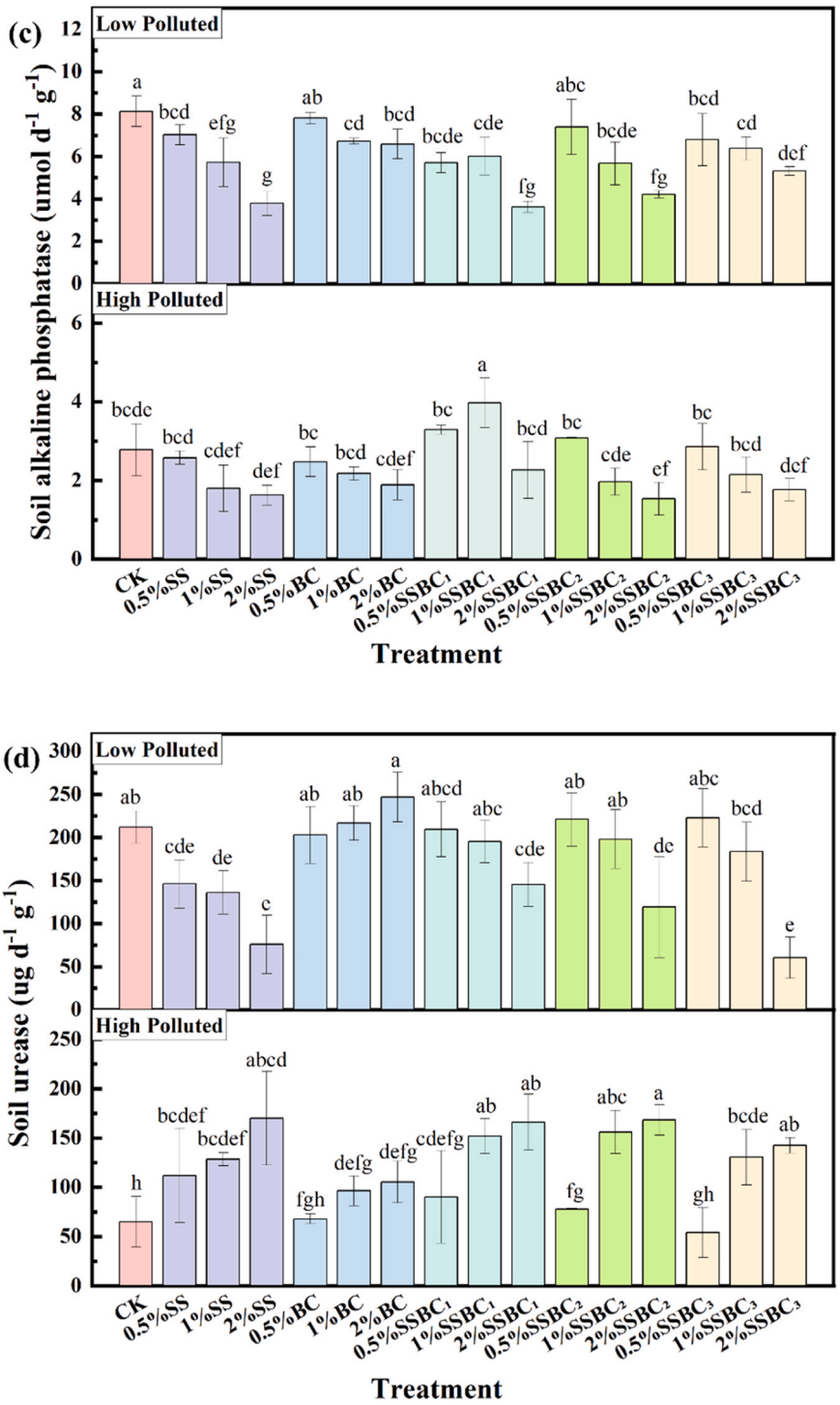


**Fig. 2.** (*continued*).

SS, $SSBC_1$, $SSBC_2$, and $SSBC_3$ treatments reduced it.

### 3.7. Adsorption kinetics

The kinetics of As(III) adsorption by the different materials are shown in Fig. 3(a). The results show that SSBCs composites reached equilibrium faster and exhibited higher adsorption capacities than either SS or BC alone. A fast adsorption rate and high adsorption capacity are critical for practical applications, as they can substantially reduce both the size and retention time required in an adsorption bed.

To further analyze the adsorption kinetics, pseudo-first-order and pseudo-second-order kinetic models were applied to fit the data, and the adsorption mechanism was partially evaluated. The pseudo-first-order model assumes that adsorption is controlled by diffusion, while the pseudo-second-order model describes chemisorption via electron sharing or transfer between the adsorbent and adsorbate. As illustrated in Fig. 3(a), the adsorption of As(III) by the five adsorbents was well described by both models. The $SSBC_1$ composite reached equilibrium within 120 min and, notably, exhibited a much faster initial adsorption rate than biochar. These results highlight that the As(III) adsorption performance of SSBCs significantly surpasses that of BC, underscoring its potential as a more effective material for pollution remediation.

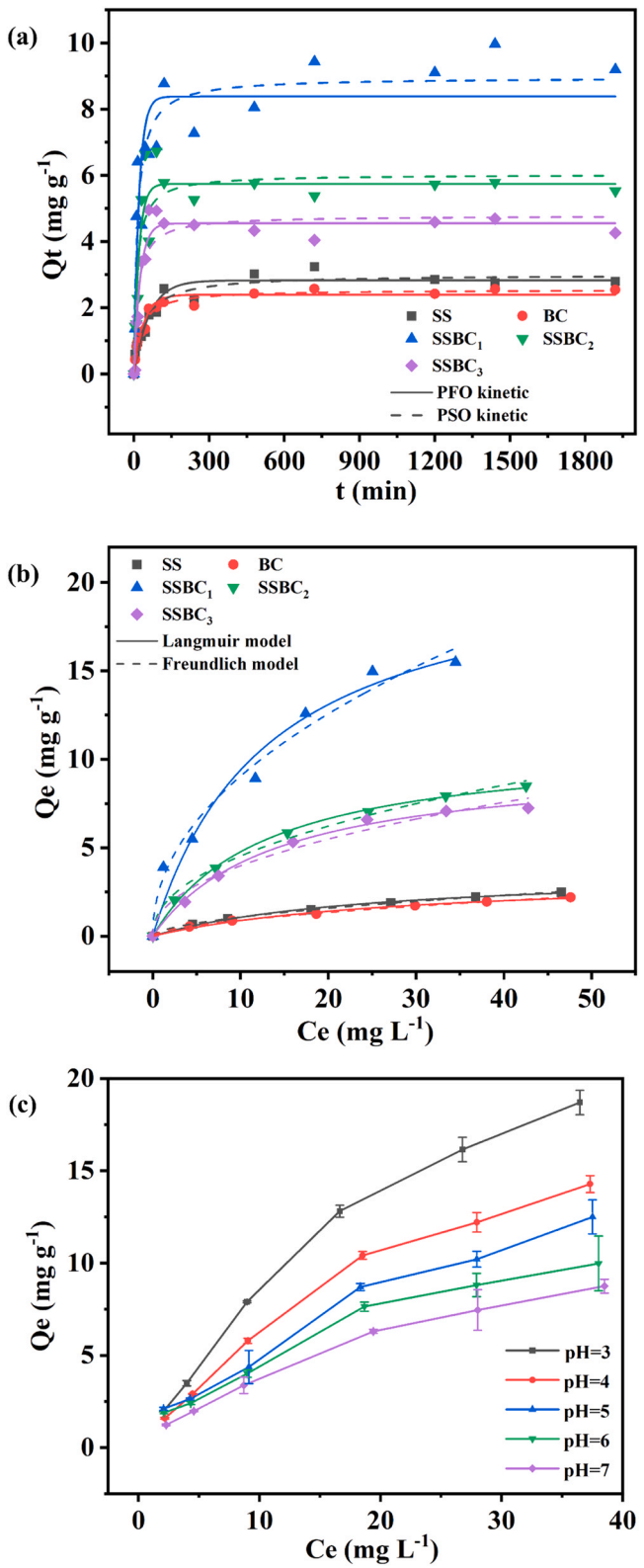


**Fig. 3.** Sorption kinetics (a) and isotherm (b) data and fitted models of As (III) on different adsorbents, and the influence of pH (c) on the adsorption by $SSBC_1$. (SS = steel slag; BC = corn straw biochar; SS and BC were mixed at mass ratios of 1:1, 2.5:1, and 10:1, labeled $SSBC_1$, $SSBC_2$, and $SSBC_3$; $Q_t$ = the adsorption capacity at time t; $Q_e$ = equilibrium adsorption capacity; $C_e$ = equilibrium concentration. Experimental conditions: adsorbent dose = 1 g $L^{-1}$, solution volume = 50 mL, pH = 7, T = 25 °C; initial As(III) concentration $C_o$ = 50 mg $L^{-1}$ for sorption kinetics).

### 3.8. Adsorption isotherms

Fig. 3(b) shows the isothermal adsorption of As(III) onto the absorbents. The data were well fitted by both Langmuir and Freundlich models ($R^2 > 0.94$; Table 3). The Langmuir model assumes adsorption occurs on a homogeneous surface with identical sites, forming a single molecular layer without interaction between adsorbed molecules (Pawar et al., 2018). In contrast, the Freundlich model describes adsorption on heterogeneous surfaces and predicts that the adsorption capacity increases with adsorbent concentration (Wang et al., 2015).

According to the Langmuir model, the maximum adsorption capacity of BC for As(III) was calculated as 3.46 mg $g^{-1}$. In comparison, the maximum adsorption capacity of $SSBC_1$ was 6.25 times higher than that of BC, while $SSBC_2$ and $SSBC_3$ showed 3.15- and 2.87-fold increases, respectively. Based on the Freundlich fitting parameters, the Freundlich constants for SSBCs ranged between 1 and 10, indicating favorable interactions between the adsorbent and heavy metal ions. These findings demonstrate that SSBCs is a much more effective adsorbent for heavy metals than biochar alone, likely because the composite provides more available adsorption sites for As(III).

### 3.9. Influence of pH on the adsorption

pH is a critical factor influencing both the surface charge of adsorbents and the speciation of As. The effect of pH on As adsorption by $SSBC_1$ is shown in Fig. 3(c). Within the pH range of 3–7, the highest adsorption of As(III) was observed at pH 3. With increasing pH, the adsorption capacity of $SSBC_1$ for As(III) decreased, a trend consistent with that reported for other adsorbents (Dong et al., 2019; Guo et al., 2015), likely due to enhanced electrostatic interactions or surface protonation.

### 3.10. Soil adsorption

To investigate the effect of adding $SSBC_1$ on the adsorption of As(III) in paddy soil, isothermal adsorption experiments were conducted using SS, BC, and $SSBC_1$. The results showed that the maximum adsorption capacity of the untreated soil (control) was 0.25 mg $g^{-1}$, while the addition of $SSBC_1$ markedly enhanced As(III) adsorption in paddy soil, with capacity increasing in response to both application rate and initial As concentration (Fig. 4(a)–c). At a 2 % application rate, $SSBC_1$ increased the maximum adsorption capacity by 31.36 %, compared with increases of 10.97 % for SS and 18.86 % for BC.

Using SS, BC, and $SSBC_1$ at a 2 % addition rate as examples, adsorption data were fitted with Langmuir and Freundlich models (Fig. 4d). Evaluation of the fitting degree using the correlation coefficient ($R^2$) (Table 4) indicated that both models provided good fits (>97 %), with the Langmuir model performing slightly better. This suggests that the surface of paddy soil provides relatively uniform adsorption sites for As(III) at low concentrations, and that adsorption mainly follows a monolayer pattern. As the initial concentration of As (III) increased, the adsorbent surface approached saturation, after which adsorption proceeded into internal sites through chemisorption. According to Table 4, the maximum adsorption capacities of As(III) in paddy soil were 0.37 mg $g^{-1}$, 0.42 mg $g^{-1}$, 0.54 mg $g^{-1}$, and 0.61 mg $g^{-1}$ for treatments without amendments and with the addition of SS, BC, and $SSBC_1$, respectively. These results confirm that $SSBC_1$ effectively improves the soil's As immobilization capacity.

## 4. Discussions

### 4.1. The regulatory mechanism of SBC on the effectiveness of As in the soil

The bioavailability of As was assessed through plant uptake in this study (Lee et al., 2025). Ryegrass was selected as the model crop to

**Table 3**
Parameters of kinetic and isotherm models for As(III) sorption onto different adsorbent materials.

| Sample | Pseudo-first-order model (PFO) | | | Pseudo-second-order model (PSO) | | | Langmuir | | | Freundlich | | |
|---|---|---|---|---|---|---|---|---|---|---|---|---|
| | $Q_e$ ($mg \cdot g^{-1}$) | $K_1$ | $R_1^2$ | $Q_e$ ($mg \cdot g^{-1}$) | $K_2$ | $R_2^2$ | $Q_m$ ($mg \cdot g^{-1}$) | $K_L$ | $R_L^2$ | $K_f$ | 1/n | $R_F^2$ |
| SS | 2.83 ± 0.12d | 0.016 ± 0.00c | 0.924 | 3.00 ± 0.12d | 0.008 ± 0.002b | 0.943 | 3.73 ± 0.26c | 0.040 ± 0.01b | 0.989 | 0.30 ± 0.012c | 0.553 ± 0.01a | 0.999 |
| BC | 2.40 ± 0.07d | 0.025 ± 0.00bc | 0.963 | 2.55 ± 0.06d | 0.015 ± 0.002a | 0.978 | 3.46 ± 0.33c | 0.034 ± 0.01b | 0.985 | 0.24 ± 0.013c | 0.580 ± 0.02a | 0.998 |
| $SSBC_1$ | 8.38 ± 0.44a | 0.049 ± 0.01a | 0.823 | 8.96 ± 0.41a | 0.008 ± 0.002b | 0.889 | 21.63 ± 3.41a | 0.077 ± 0.03a | 0.944 | 3.03 ± 0.480a | 0.474 ± 0.05b | 0.978 |
| $SSBC_2$ | 5.74 ± 0.26b | 0.050 ± 0.011a | 0.878 | 6.03 ± 0.37b | 0.012 ± 0.005ab | 0.823 | 10.93 ± 0.37b | 0.077 ± 0.01a | 0.994 | 1.58 ± 0.151b | 0.457 ± 0.03b | 0.992 |
| $SSBC_3$ | 4.54 ± 0.14c | 0.040 ± 0.01ab | 0.949 | 4.76 ± 0.25c | 0.012 ± 0.004ab | 0.889 | 9.92 ± 0.43b | 0.071 ± 0.01a | 0.991 | 1.36 ± 0.265b | 0.463 ± 0.06b | 0.971 |

Note: CK is control (no amendment); SS is steel slag; BC is corn straw biochar; SS and BC were mixed at mass ratios of 1:1, 2.5:1, and 10:1, labeled $SSBC_1$, $SSBC_2$, and $SSBC_3$, different letters indicate significant differences at $p < 0.05$; the same letter indicates no significant difference.

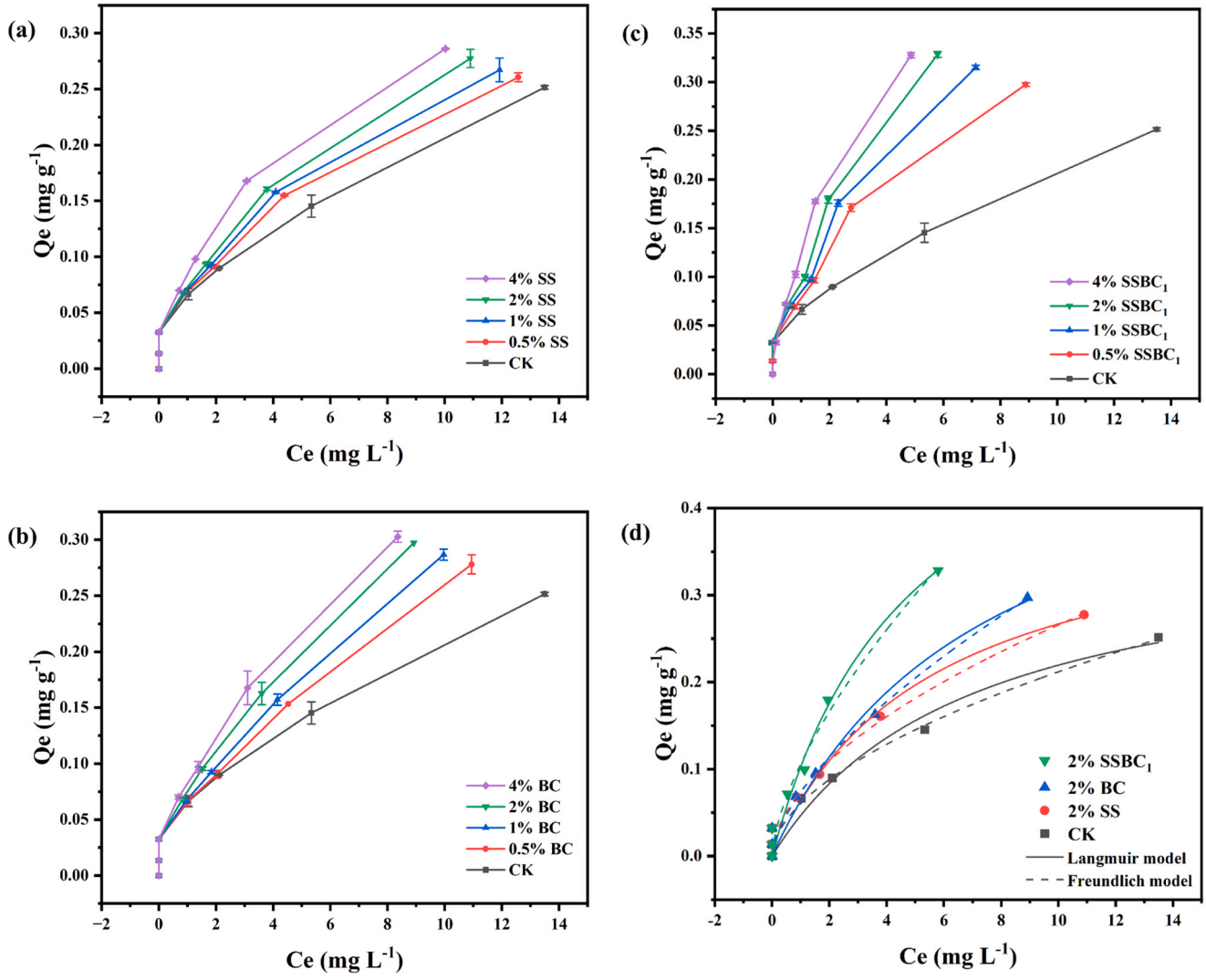


**Fig. 4.** Effects of different material additions on the adsorption of As(III) in paddy soil: (a) SS (steel slag); (b) BC (corn straw biochar); (c) $SSBC_1$ (SS and BC were mixed at mass ratios of 1:1); (d) adsorption isotherm fitting curves for paddy soil with 2 % different adsorption materials ($Q_e$ = equilibrium adsorption capacity; $C_e$ = equilibrium concentration. Experimental conditions: adsorbent dose = 1 g $L^{-1}$, solution volume = 50 mL, pH = 7, T = 25 °C).

evaluate the effect of SSBCs on As accumulation in contaminated soil. The results showed that SSBCs application significantly reduced As concentrations in different tissues of ryegrass, while simultaneously enhancing crop yield and promoting overall plant growth. Previous studies have demonstrated that biochar can act as both a nutrient and carbon source, thereby improving growth and physiological functions of plants cultivated in As-contaminated soils (Li, Zhang, et al., 2021). The reduction in As accumulation observed in ryegrass following SSBCs application can largely be attributed to improvements in soil physico-chemical properties and increased Fe and Ca oxide contents, which play

**Table 4**
Isothermal adsorption fitting parameters for As(III) adsorption of in paddy soil with different additives.

| Sample | Langmuir | | | Freundlich | | |
|---|---|---|---|---|---|---|
| | Qm ($mg \cdot g^{-1}$) | $K_L$ | $R_L^2$ | $K_f$ | 1/n | $R_F^2$ |
| CK | 0.37 ± 0.067c | 0.144 ± 0.055a | 0.978 | 0.06 ± 0.010b | 0.546 ± 0.071a | 0.973 |
| SS | 0.42 ± 0.029bc | 0.180 ± 0.036a | 0.991 | 0.07 ± 0.010b | 0.552 ± 0.063a | 0.978 |
| BC | 0.54 ± 0.010b | 0.135 ± 0.040a | 0.987 | 0.07 ± 0.009b | 0.637 ± 0.068a | 0.981 |
| $SSBC_1$ | 0.61 ± 0.026a | 0.204 ± 0.051a | 0.990 | 0.11 ± 0.011a | 0.648 ± 0.070a | 0.979 |

Note: CK is control (no amendment); SS is steel slag; BC is corn straw biochar; $SSBC_1$ is SS and BC were mixed at mass ratios of 1:1, different letters indicate significant differences at $p < 0.05$; the same letter indicates no significant difference.

key roles in As transformation and plant growth. Critically, the superior performance of SSBCs compared with their raw precursors arises from the synergistic integration of the porous BC matrix with SS-derived reactive phases. XPS and FTIR analyses (Supporting Information, Figs. S2–S3) confirmed the presence of Fe- and Ca-bearing phases and their successful incorporation into the SSBC matrix. These Fe/Ca oxides are essential because they provide specific adsorption sites that are largely absent in BC alone, while the BC component helps mitigate the excessive pH increase and poor porosity typically associated with SS. This synergy is reflected in the optimal pH and highest surface area observed for $SSBC_1$ (Table S1). These findings are consistent with earlier reports showing that Fe- and Ca-based oxides effectively reduce As uptake by ryegrass (Arco-Lázaro et al., 2018; Cao et al., 2024; Gutierrez et al., 2010). Similarly, Qiao et al. (2018) found that ZVI-BC significantly decreased soil As bioavailability while increasing the immobilized fraction of As. Additionally, various soil factors, including pH, active organic matter content, and available As levels, may also influence As absorption by ryegrass (Liu et al., 2020; Wang et al., 2024; Zhang et al., 2023).

Soil pH is a critical factor influencing the bioavailability of heavy metals. In this study, both types of As-contaminated soils were weakly acidic, with higher contamination levels corresponding to greater acidity. Because SSBCs were alkaline materials, their application led to a significant increase in soil pH. The magnitude of this increase followed the order SS > SSBCs > BC, indicating that the composite effectively moderated the strong alkalinity of raw SS. This buffering effect was advantageous for both plant growth and microbial functioning, as reflected in the biomass and enzyme activity results. The pH moderation arose from the composite's structural design, in which the BC matrix incorporated and regulated the alkaline components derived from SS. The elevated soil pH also altered arsenic speciation and increased the negative charge on soil particle surfaces, thereby enhancing electrostatic repulsion and influencing As desorption behavior. (Fan et al., 2020). Previous research has shown that a soil pH range of 7–8 is favorable for As immobilization (Wang et al., 2014). The alkaline oxides in SSBCs, such as Ca–O, Fe–O, Mg–O, and Si–O, identified via material characterization, can react with soil moisture to release hydroxide ions ($OH^-$), directly increasing soil pH (Zaw et al., 2022). Guofei Liu et al. (2020) reported that the application of biochar (resulting in a soil pH of 5.9) and calcium carbide slag (resulting in a soil pH of 6.53) at the split-leaf stage increased soil pH by 0.51 and 1.14 units, respectively. Because calcium carbide slag mainly consists of calcium and magnesium oxides, it exerts the strongest effect on elevating soil pH. The rise in pH may also enhance metal adsorption capacity and promote the formation of insoluble precipitates (Kolodynska et al., 2012). Hydroxyl groups (–OH) on the surface of SSBCs can react with hydrogen ions ($H^+$), while released $Ca^{2+}$ and $Mg^{2+}$ ions can further neutralize acidity through ion-exchange processes. Similarly, Ibrahim et al. (2017) demonstrated in pot experiments using sludge-derived biochar and peanut shell biochar that biochar application effectively increased soil pH, aligning with our findings. It should be noted that arsenate anion adsorption can increase under acidic conditions due to the behavior of variable-charge soil minerals (Caporale and Violante, 2016). However, Liu et al. (2020) also found that although the application of three different amendments raised soil pH and increased soil negative charge, the bioavailability of As in the soil did not increase. This highlights the complexity of pH-driven effects on As dynamics in soil. Active organic matter constitutes a crucial component of soil, representing the fraction of organic matter with higher biological activity. It serves as a direct nutrient source for plants and influences nutrient uptake and utilization (Adhikari and Hartemink, 2016). In this study, the application of SSBCs enhanced soil organic matter activity. This improvement can be attributed to the material's high organic carbon content, which increases soil organic matter levels (Van Zwieten et al., 2010), as well as its ability to form complexes with As, thereby promoting As adsorption and fixation in the soil and reducing its mobility and transformation potential (Aftabtalab et al., 2022; Uchimiya et al., 2013). The well-developed porous structure of SSBCs, reflected in their high adsorption capacity, likely further enhanced their ability to retain organic matter and associated As complexes within the soil matrix.

The available As content in soil refers to the fraction of As that can be absorbed and utilized by plants during ecological migration processes. In general, As oxyanions in soil can be immobilized through physical mechanisms (e.g., pore filling and electrostatic adsorption) and chemical mechanisms (e.g., complexation and co-precipitation) involving metal (hydrated) oxides (Wan et al., 2020). This study showed that SSBCs application significantly reduced available As in soil and mitigated As uptake by ryegrass. The SSBCs achieved this not only through general mechanisms such as pore filling, supported by their high BET surface area (Table S1) and electrostatic adsorption, but more importantly through enhanced chemical immobilization derived from their composite nature. The presence of Fe–O and Ca–O functional groups, confirmed by FTIR (Fig. S2), enabled specific complexation and precipitation reactions (e.g., formation of Fe–As and Ca–As precipitates). These mechanisms were far less pronounced in BC and were less efficiently utilized in SS due to its comparatively lower surface area. This effect is primarily attributed to the ability of As to form hydrogen bonds with surface functional groups of SSBCs, such as –OH, C═O, C–O, Fe–O, and Ca–O, thereby enhancing its retention in the soil matrix and reducing bioavailability(Wei et al., 2024; Zaw et al., 2022). Previous studies have indicated that amendments combining steel slag (SS) with ferrous sulfate ($FeSO_4$) can effectively reduce As availability in mineralized soils. This is mainly due to the adsorption of As by inorganic $Fe^{3+}$ oxides and free $Ca^{2+}$ ions generated during reactions, leading to the formation of Fe–As and Ca–As precipitates that enhance As immobilization (Zhang et al., 2023). Seyfferth et al. (2019) similarly reported that As can be immobilized via binding to iron oxides and co-precipitation. In addition, As may form complexes with oxygen-containing functional groups or protonated carbon species (e.g., –COOH and C═O) on the biochar surface through complexation reactions, a mechanism consistent with findings from of this study (K. Liu et al., 2020; Yang et al., 2024). Beyond chemical adsorption mechanisms, Wei et al. (2025) revealed that the As fixation capacity of an electrolytic manganese slag-biochar composite material (EB) is largely due to its high specific surface area (SSA), which facilitates the interaction through pore-filling effects, as evidenced by EDS analysis. Their results indicated that As was adsorbed onto the surface of EB, thereby reducing its uptake by lettuce. Physicochemical characterizations of the SSBCs, including SEM imaging and BET pore structure analysis, are provided in the Supporting Information (Fig. S1 and Table S1). These analyses showed that $SSBC_1$ possessed a well-developed porous structure, consistent with its enhanced adsorption capacity. This structural feature may facilitate the physical entrapment of As within soil pores, complementing the chemical immobilization mechanisms described above. Overall, these

findings demonstrate that As concentrations in ryegrass are closely correlated with the available As content in soil, highlighting the regulatory role of SSBCs in reducing As bioavailability.

Soil enzymes play a vital role in nutrient cycling and are actively involved in key biochemical processes within the soil (Cao et al., 2017). Previous studies have shown that enzyme activity is highly sensitive to As contamination (Aponte et al., 2020). Enzymes such as peroxidase, urease, and phosphatase are particularly vulnerable to As exposure. Two primary mechanisms may explain this effect: (i) As can directly interact with soil enzymes by binding to sulfur-containing functional groups, thereby potentially inhibiting enzymatic activity; and (ii) As can indirectly alter the abundance and types of enzymes secreted by soil microorganisms by influencing microbial community composition and activity, ultimately leading to changes in enzyme activity (Ciarkowska, 2015; Jin et al., 2024). As a result, soil enzyme activity generally declines with increasing As pollution. Beyond As contamination, other soil properties—including pH and active organic matter content—also affect enzyme activity (Ning et al., 2025; Wang et al., 2013). SSBCs, characterized by its well-developed pore structure, high carbon content, and metal–oxygen functional groups, can modify soil physicochemical properties and thereby likely influence enzyme activity. Thus, the application of SSBCs not only reduces available As in soil but also may help mitigate the negative impacts of As on soil enzyme activity.

Soil catalase (S-CAT) is involved in redox reactions and is widely used as an indicator of aerobic microbial abundance and soil fertility (Zheng et al., 2017). In this study, S-CAT activity increased in treatments amended with SSBCs. This enhancement suggested that oxidative stress in the soil was alleviated, which could indirectly indicate that SSBCs reduced the bioavailability of As and alleviated its toxic effects on ryegrass.

Soil peroxidase (S-POD), another important antioxidant enzyme, contributes to both the synthesis and degradation of soil organic matter and plays an essential role in the carbon cycle (Garbuz et al., 2023). Results showed that SSBCs application significantly increased S-POD activity in the low-As soils. This response may be linked to mild As stress inducing a “stress adaptation” mechanism in microorganisms, up-regulating S-POD expression to enhance antioxidant capacity (Nabi et al., 2019). Conversely, in the high-As soils, SSBCs application suppressed S-POD activity. This inhibition could be attributed to competition between minerals released from the SSBCs and either As or enzyme molecules for adsorption sites, or to changes in soil colloid surface charge that alter S-POD adsorption and catalytic efficiency (Prayogo et al., 2014).

Soil alkaline phosphatase (S-AKP) is essential for phosphorus cycling in soil (C. Y. Liu et al., 2019). Previous studies have demonstrated that S-AKP is particularly sensitive to heavy metal toxicity, with its activity often being suppressed (Li et al., 2017). In this study, higher SSBCs application rates were associated with decreased S-AKP activity. This may be due to the adsorption of alkaline phosphatase by BC, with the extent of adsorption potentially positively correlated with the degree of enzyme activity inhibition (Khadem and Raiesi, 2019). These results are consistent with observations reported by Zhang et al. (2017).

S-UE, a specific hydrolase in soil, catalyzes the hydrolysis of urea and is commonly used as a biomarker for assessing heavy metal toxicity (Tan et al., 2022). In this study, increasing SSBCs dosage reduced urease activity in low-As soils but enhanced it in high-As soils. In low-As environments, the limited bioavailability of As results in minimal direct toxicity to microorganisms and urease. One possible explanation is that because SSBCs were rich in carbon but contains little nitrogen, its addition may induce a carbon–nitrogen imbalance, reducing available nitrogen and thereby potentially inhibiting urease synthesis. Moreover, the strong adsorption capacity of SSBCs may sequester both available nitrogen and urea molecules, interfering with urease function (Jin et al., 2024; Prayogo et al., 2014). In contrast, in high-As soils, SSBCs likely reduced As bioavailability, alleviated its toxic effects on microbial communities, and consequently may have promoted urease activity. Similar dual effects have been reported in other studies (Huang et al., 2017; Oladele, 2019).

In conclusion, SSBCs effectively enhance the immobilization of As in soil, thereby reducing the risk of its transfer to ryegrass. The underlying mechanism likely involves the specific material properties of SSBCs (e.g., functional groups, metal oxides, alkalinity, porosity) enabling improvement of soil physicochemical properties and the regulation of soil enzyme activity, which together influence the bioavailability of As.

### 4.2. Adsorption mechanism of S-BC for As

The previous discussion centered on the regulatory mechanism of SSBCs in modulating As bioavailability in contaminated soil during pot experiments with ryegrass. In this study, adsorption experiments combined with material characterization were used to further elucidate the mechanisms underlying As removal, providing a theoretical basis for the remediation of As-contaminated soils. Based on adsorption kinetics and isothermal model results, which revealed that SSBC$_1$ possessed a substantially higher adsorption capacity than either BC or SS (Table 3), changes in the functional groups and valence states of As(III) before and after adsorption onto the composite biochar were analyzed using FTIR and XPS to elucidate the underlying mechanisms for this enhancement.

The FTIR spectra of SSBC$_1$ before and after As(III) adsorption are shown in Fig. 5(a). Comparative analysis revealed only slight differences in the types of functional groups present, but with reduced peak intensities in some regions. The bands corresponding to hydroxyl (–OH), C–O, and Ca–O groups at 3423, 1041, and 1423 cm$^{-1}$ (Li et al., 2020; Shao et al., 2020) shifted after adsorption, indicating that these groups participated in As(III) binding through surface complexation and chemical adsorption. Moreover, the intensity of –OH bands increased, suggesting that additional –OH groups were introduced after As(III) adsorption. A significant enhancement and broadening of Fe–O peaks at 572.43 cm$^{-1}$ (Liyun et al., 2022) indicated strong interactions between As and Fe–O groups. In contrast, the Ca–O peaks at 1423 and 873 cm$^{-1}$ decreased markedly, suggesting that Ca–O groups participated in precipitation reactions with As(III). These changes provide direct evidence that the SS-derived components serve as the primary sites for chemical adsorption and precipitation, thereby explaining the superior performance of the composite compared with BC alone. These observations are consistent with the findings of Ning et al. (2016), who reported that SS containing CaO, FeO, and SiO exhibits strong adsorption and precipitation capacities. In summary, electrostatic adsorption and surface complexation represent the dominant mechanisms for As(III) removal by SSBC$_1$, with surface functional groups playing a critical role in controlling its adsorption properties. Identifying these mechanisms in the aqueous phase provides an essential foundation for interpreting the performance of SSBCs within the more complex soil system of the pot experiment.

Using XPS to analyze the variations in functional groups before and after As(III) adsorption, we further explored the adsorption mechanism of SSBC$_1$ (Fig. 5). The survey spectra (Fig. 5b, S3) confirm the incorporation of Fe and Ca from SS into the composite. The C1s spectrum (Fig. 5(c)) of SSBC$_1$ displayed three major peaks at 289.68, 285.74, and 284.14 eV, corresponding to C═O, C–O, and C═C, respectively. After As(III) adsorption, the three peaks shifted slightly to 289.22, 285.54, and 284.15 eV, indicating interactions between carbon functional groups and As. The O1s spectrum (Fig. 5(d)) was deconvoluted into four peaks based on binding energies: C–O (533.80 eV), Ca–O (532.80 eV), –OH (531.55 eV), and Fe–O (531.90 eV) (Hu et al., 2015). The proportion of –OH groups increased from 12.5 % before adsorption to 21.88 % after adsorption, highlighting the significant role of hydroxyl groups in As binding. Variations in the intensities of Ca–O and Fe–O peaks before and after adsorption suggest their involvement in the transformation of As(III) to As(V). Moreover, the Fe2p spectrum (Fig. 5(e)) shifted to higher binding energy following adsorption, consistent with the formation of Fe–O–As complexes. Lin et al. (2019)also reported that Fe–O

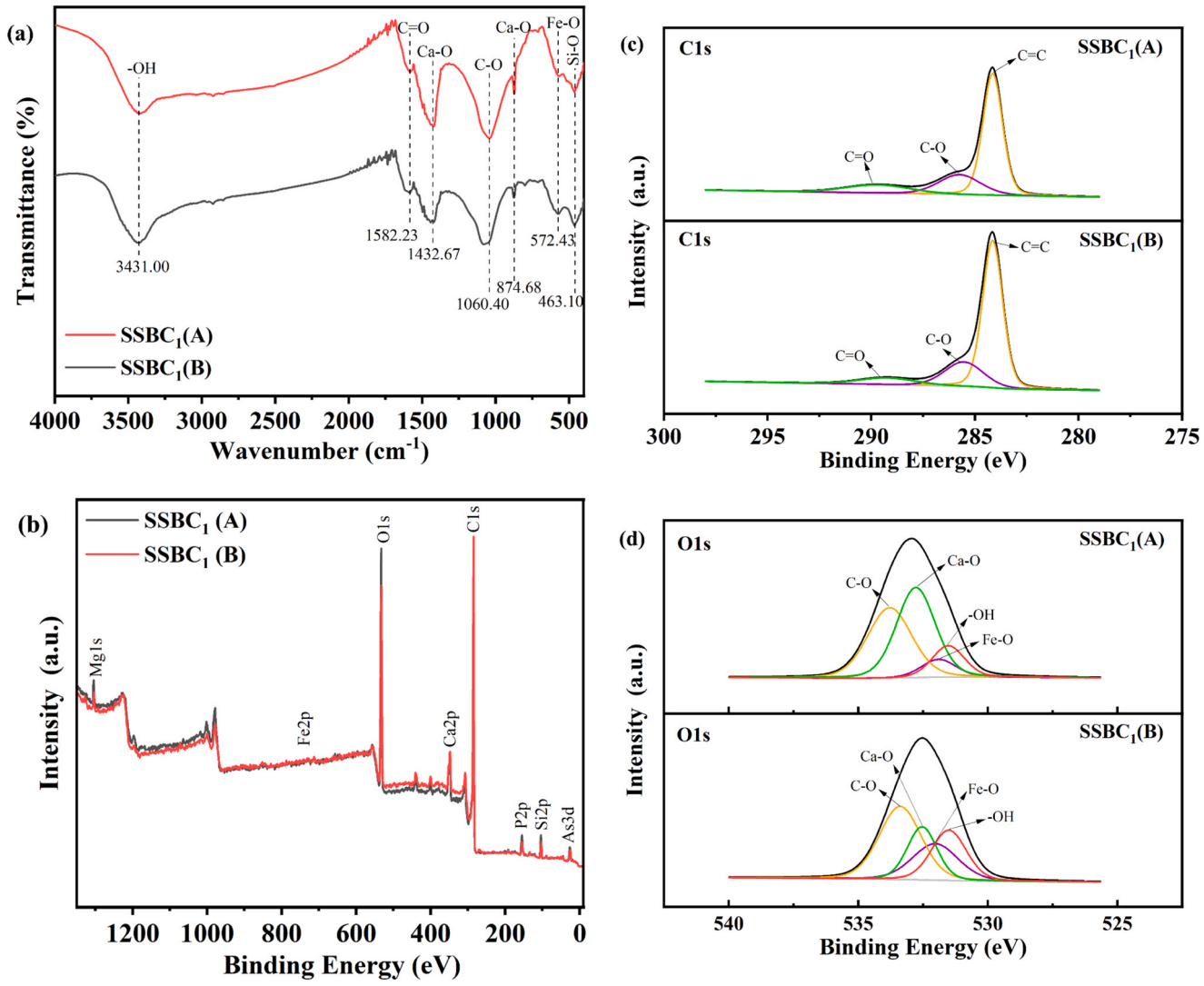


**Fig. 5.** FTIR and XPS spectra of SSBC₁ before and after As(III) adsorption. (a) FTIR; (b) XPS Survey Spectrum; (c) C1s; (d) O1s; (e) Fe2p; (f) As3d. (SSBC₁ = SS and BC were mixed at mass ratios of 1:1. A represents SSBC₁ before As(III) adsorption; B represents SSBC₁ after As(III) adsorption).

plays a crucial role in As adsorption. Following As(III) adsorption, the As3d peak spectrum (Fig. 5(f)) appeared, confirming the presence of As on SSBC₁. Two distinct peaks were observed at approximately 45.6 eV and 44.4 eV, corresponding to As(V) and As(III), respectively (Liu et al., 2019). Quantitative analysis indicated that As(V) accounted for 69.57 % of the total As, while As(III) represented 30.43 %, suggesting partial oxidation of As(III) to As(V) during adsorption. This oxidation represented a key mechanistic advantage of SSBCs over their individual components, contributing to more stable and effective As immobilization. The overall mechanism can be described as initial electrostatic adsorption of As(III), followed by partial oxidation to As(V), with the oxidized species subsequently retained on the adsorbent. These findings confirm that the synergistic action of Fe–O, Ca–O, and –OH functional groups drives the immobilization of As(III), with electrostatic adsorption and surface complexation serving as the principal mechanisms of adsorption on SSBC₁. This detailed mechanistic understanding, derived from controlled experimental studies, strongly supports the hypothesis that similar processes including As binding to functional groups, oxidation, and precipitation, contributed to the reduced As bioavailability and plant uptake observed in the pot experiment. The composite nature of SSBCs, integrating the key reactive components of SS and BC, produced a material with enhanced and multifunctional adsorption sites, which explained its superior performance compared with the individual precursors in both aqueous and soil environments. Furthermore, the persistence of these mechanisms under soil conditions, although potentially influenced by soil constituents was reflected in the consistent trends observed in soil As availability, plant As accumulation, and associated changes in soil chemistry reported in Section 4.1.

## 5. Conclusions

This study utilized low-cost solid waste steel slag together with agricultural residue corn straw to prepare SSBCs that demonstrated superior adsorption performance. Incorporation of SSBCs into As-contaminated soil promoted ryegrass biomass growth. Compared with the control and raw material treatment groups, SSBCs effectively reduced As accumulation in different tissues of ryegrass. In soils with low and high As contamination, the addition of 2 % SSBC₁ decreased available As concentrations by 55.51 % and 28.38 %, respectively. This not only lowered As bioavailability but also increased active organic matter content and enhanced soil enzyme activity. Kinetic and isothermal adsorption analyses demonstrated that SSBC₁ reached adsorption equilibrium within approximately 2 h. Langmuir isotherm fitting further indicated that the maximum adsorption capacity was

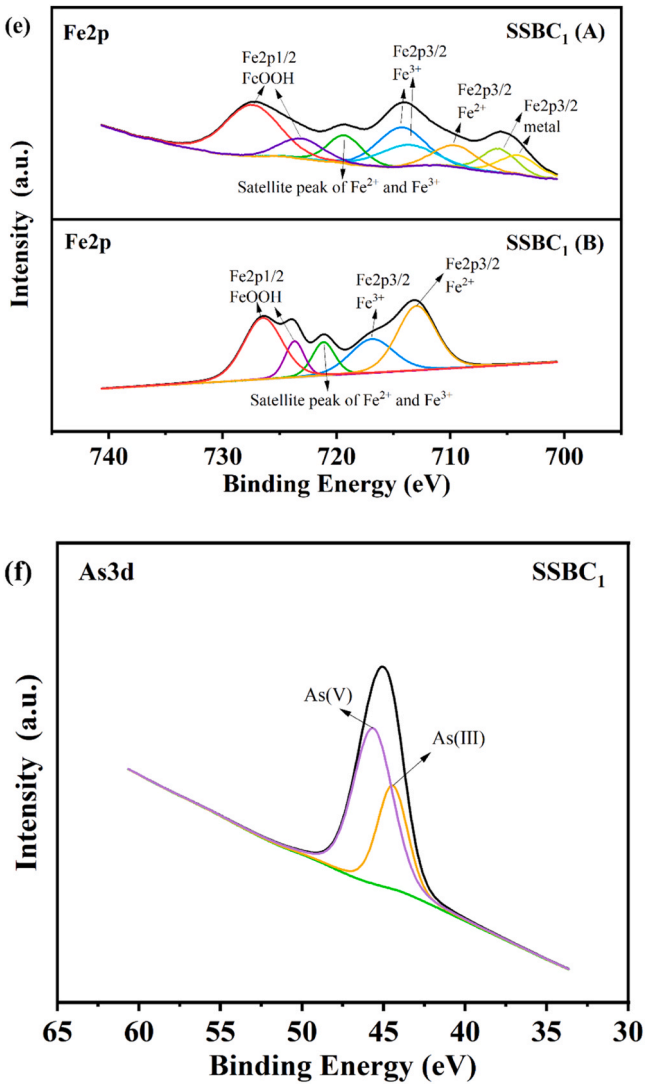


**Fig. 5.** (*continued*).

21.63 mg $g^{-1}$ . Additionally, low solution pH significantly enhanced the adsorption efficiency of $SSBC_1$ for As(III), thereby promoting As adsorption in soil. Overall, this study demonstrates a "waste-treats-waste" strategy by converting steel slag and corn straw into an efficient immobilization agent for As in soil. $SSBC_1$ functions as an effective immobilization material for reducing As bioavailability in soil, offering important potential for soil remediation.

## CRediT authorship contribution statement

**Zhengguo Song:** Writing – original draft, Supervision, Project administration, Funding acquisition. **Cheng Qiu:** Supervision, Project administration, Funding acquisition. **Youming Dong:** Writing – original draft, Supervision, Investigation. **Weiwen Qiu:** Data curation. **Minling Gao:** Formal analysis, Data curation. **Xuemei Yang:** Writing – original draft, Investigation, Data curation.

## Declaration of Competing Interest

The authors declare that they have no known competing financial interests or personal relationships that could have appeared to influence the work reported in this paper.

## Acknowledgement

This work was financially supported by the earmarked fund for CARS-05, the Innovation Team Project of Guangdong Provincial Department of Education, China 2023KCXTD012), Guangdong Natural Science Foundation (No. 2023A1515110486), and Key scientific and technological research topics of Xizang (No. XZ202501ZY0028).

## Appendix A. Supporting information

Supplementary data associated with this article can be found in the online version at doi:10.1016/j.indcrop.2025.122464.

## Data availability

The authors do not have permission to share data.

## References

Adhikari, K., Hartemink, A.E., 2016. Linking soils to ecosystem services - A global review. Geoderma 262, 101–111. https://doi.org/10.1016/j.geoderma.2015.08.009.

Aftabtalab, A., Rinklebe, J., Shaheen, S.M., Niazi, N.K., Moreno-Jimenez, E., Schaller, J., Knorr, K.H., 2022. Review on the interactions of arsenic, iron (oxy)(hydr)oxides, and dissolved organic matter in soils, sediments, and groundwater in a ternary system.

Article 131790 Chemosphere 286. https://doi.org/10.1016/j.chemosphere.2021.131790.
Aponte, H., Meli, P., Butler, B., Paolini, J., Matus, F., Merino, C., Kuzyakov, Y., 2020. Meta-analysis of heavy metal effects on soil enzyme activities. Article 139744 Sci. Total Environ. 737. https://doi.org/10.1016/j.scitotenv.2020.139744.
Arco-Lázaro, E., Pardo, T., Clemente, R., Bernal, M.P., 2018. Arsenic adsorption and plant availability in an agricultural soil irrigated with As-rich water: effects of Fe-rich amendments and organic and inorganic fertilisers. J. Environ. Manag. 209, 262–272. https://doi.org/10.1016/j.jenvman.2017.12.042.
Boyd, S., Mortland, M., 2017. 1 Enzyme interactions with clays and clay-organic matter complexes. Soil Biochem.
Cao, Q., Steinman, A.D., Su, X.M., Xie, L.Q., 2017. Effects of microcystins contamination on soil enzyme activities and microbial community in two typical lakeside soils. Environ. Pollut. 231, 134–142. https://doi.org/10.1016/j.envpol.2017.08.013.
Cao, J., Tan, Y.P., Zhang, C.X., 2024. Combined approaches for the remediation of cadmium- and arsenic-contaminated soil: phytoremediation and stabilization strategies. Article 7144 Appl. Sci. 14 (16). https://doi.org/10.3390/app14167144.
Caporale, A.G., Violante, A., 2016. Chemical processes affecting the mobility of heavy metals and metalloids in soil environments. Curr. Pollut. Rep. 2 (1), 15–27. https://doi.org/10.1007/s40726-015-0024-y.
Chen, G.N., Du, Y.H., Fang, L.P., Wang, X.Q., Liu, C.P., Yu, H.Y., Li, F.B., 2023. Distinct arsenic uptake feature in rice reveals the importance of N fertilization strategies. Article 158801 Sci. Total Environ. 854. https://doi.org/10.1016/j.scitotenv.2022.158801.
Ciarkowska, K., 2015. Enzyme activities in soils contaminated with heavy metals in varying degrees. Heavy Met. Contam. Soils 145–158. https://doi.org/10.1007/978-3-319-14526-6_8.
Dan, Y.T., Wang, X.X., Ji, M.Y., Sang, W.J., Shen, Z., Zhang, Y.L., 2023. Influence of temperature change on the immobilization of soil Pb and Zn by hydrochar: roles of soil microbial modulation. Article 121109 Environ. Pollut. 320. https://doi.org/10.1016/j.envpol.2023.121109.
Dippenaar, R., 2005. Industrial uses of slag (the use and re-use of iron and steelmaking slags). Ironmak. Steelmaking 32 (1), 35–46. https://doi.org/10.1179/174328105X15805.
Dong, Y.M., Gao, M.L., Song, Z.G., Qiu, W.W., 2019. Adsorption mechanism of As(III) on polytetrafluoroethylene particles of different size. Article 112950 Environ. Pollut. 254. https://doi.org/10.1016/j.envpol.2019.07.118.
Fan, J., Chen, X., Xu, Z.B., Xu, X.Y., Zhao, L., Qiu, H., Cao, X.D., 2020. One-pot synthesis of nZVI-embedded biochar for remediation of two mining arsenic-contaminated soils: arsenic immobilization associated with iron transformation. Article 122901 J. Hazard. Mater. 398. https://doi.org/10.1016/j.jhazmat.2020.122901.
Gadd, G.M., 2009. Arsenic pollution: a global synthesis. Exp. Agricul. 45 (4), 509-509.
Garbuz, S., Mackay, A., Camps-Arbestain, M., DeVantier, B., Minor, M., 2023. Biochar increases soil enzyme activities in two contrasting pastoral soils under different grazing management. Crop pasture Sci. 74 (2), 101–111. https://doi.org/10.1071/CP21790.
Gong, Y., Qu, Y., Yang, S., Tao, S., Shi, T., Liu, Q., Ma, J., 2020. Status of arsenic accumulation in agricultural soils across China (1985–2016). Environ. Res. 186, 109525. https://doi.org/10.1016/j.envres.2020.109525.
Guo, J.L., Bao, Y.P., Wang, M., 2018. Steel slag in China: treatment, recycling, and management. Waste Manag. 78, 318–330. https://doi.org/10.1016/j.wasman.2018.04.045.
Guo, L.Q., Ye, P.R., Wang, J., Fu, F.F., Wu, Z.J., 2015. Three-dimensional Fe3O4-graphene macroscopic composites for arsenic and arsenate removal. J. Hazard. Mater. 298, 28–35. https://doi.org/10.1016/j.jhazmat.2015.05.011.
Gutierrez, J., Hong, C.O., Lee, B.H., Kim, P.J., 2010. Effect of steel-making slag as a soil amendment on arsenic uptake by radish (Raphanus sativa L.) in an upland soil. Biol. Fertil. Soils 46 (6), 617–623. https://doi.org/10.1007/s00374-010-0470-z.
Hu, X., Ding, Z., Zimmerman, A.R., Wang, S., Gao, B., 2015. Batch and column sorption of arsenic onto iron-impregnated biochar synthesized through hydrolysis. Water Res. 68, 206–216. https://doi.org/10.1016/j.watres.2014.10.009.
Huang, M., Zhou, X.F., Chen, J.N., Cao, F.B., Jiang, L.G., Zou, Y.B., 2017. Interaction of changes in pH and urease activity induced by biochar addition affects ammonia volatilization on an acid paddy soil following application of urea. Commun. Soil Sci. Plant Anal. 48 (1), 107–112. https://doi.org/10.1080/00103624.2016.1253725.
Hunting, W.M., Gagnon, M., Esselen, W.B., 1959. New method for peroxidase determination. Anal. Chem. 9 (1), 143–144.
Ibrahim, M., Li, G., Khan, S., Chi, Q.Q., Xu, Y.Y., 2017. Biochars mitigate greenhouse gas emissions and bioaccumulation of potentially toxic elements and arsenic speciation in Phaseolus vulgaris L. Environ. Sci. Pollut. Res. 24 (24), 19524–19534. https://doi.org/10.1007/s11356-017-9605-1.
Jin, H.M., Capareda, S., Chang, Z.Z., Gao, J., Xu, Y.D., Zhang, J.Y., 2014. Biochar pyrolytically produced from municipal solid wastes for aqueous As(V) removal: adsorption property and its improvement with KOH activation. Bioresour. Technol. 169, 622–629. https://doi.org/10.1016/j.biortech.2014.06.103.
Jin, K., Sleutel, S., Buchan, D., Neve, S.D., Cai, D.X., Gabriels, D., Jin, J.Y., 2009. Changes of soil enzyme activities under different tillage practices in the Chinese Loess Plateau. Soil Tillage Res. 104 (1), 115–120.
Jin, X.X., Zhang, T.X., Hou, Y.T., Bol, R., Zhang, X.J., Zhang, M., Wang, J.K., 2024. Review on the effects of biochar amendment on soil microorganisms and enzyme activity. J. Soils Sediment. 24 (7), 2599–2612. https://doi.org/10.1007/s11368-024-03841-7.
Kandeler, E., Gerber, H., 1988. Short-term assay of soil urease activity using colorimetric determination of ammonium. Biol. Fertil. Soils 6 (1), 68–72.
Kapoor, R.T., Hasanuzzaman, M., 2024. Unlocking the potential of co-application of steel slag and biochar in mitigation of arsenic-induced oxidative stress by modulating antioxidant and glyoxalase system in Abelmoschus esculentus L. Chemosphere 351 (000).
Khadem, A., Raiesi, F., 2019. Response of soil alkaline phosphatase to biochar amendments: Changes in kinetic and thermodynamic characteristics. Geoderma 337, 44–54. https://doi.org/10.1016/j.geoderma.2018.09.001.
Khan, Z.H., Gao, M.L., Qiu, W.W., Song, Z.G., 2020. Efficient As(III) removal by novel MoS2-impregnated Fe-oxide-biochar composites: characterization and mechanisms. ACS Omega 5 (22), 13224–13235. https://doi.org/10.1021/acsomega.0c01268.
Kim, S.H., Chung, H., Jeong, S., Nam, K., 2021. Identification of pH-dependent removal mechanisms of lead and arsenic by basic oxygen furnace slag: relative contribution of precipitation and adsorption. Article 123451 J. Clean. Prod. 279. https://doi.org/10.1016/j.jclepro.2020.123451.
Kolodynska, D., Wnetrzak, R., Leahy, J.J., Hayes, M.H.B., Kwapinski, W., Hubicki, Z., 2012. Kinetic and adsorptive characterization of biochar in metal ions removal. Chem. Eng. J. 197, 295–305. https://doi.org/10.1016/j.cej.2012.05.025.
Lee, J., Seo, M., Cho, W., Lee, J.Y., 2025. The effect of heavy metal stabilizers in arsenic-contaminated soil: using bioavailability. J. Mater. Cycles Waste Manag. 27 (2), 746–760. https://doi.org/10.1007/s10163-024-02155-7.
LEFROY, R.D.B., BLAIR, G.J., STRONG, W.M., 1993. Changes in soil organic-matter with cropping as measured by organic-carbon fractions and C-13 natural isotope abundance. Dev plant soil sci.
Lehmann, J., Joseph, S., 2009. Biochar for environmental management:science, technology and implementation. Taylor Fr. https://doi.org/10.4324/9781003297673.
Li, B.T., Chen, Y.R., Liang, W.Z., Mu, L.L., Bridges, W.C., Jacobson, A.R., Darnault, C.J. G., 2017. Influence of cerium oxide nanoparticles on the soil enzyme activities in a soil-grass microcosm system. Geoderma 299, 54–62. https://doi.org/10.1016/j.geoderma.2017.03.027.
Li, Qi, X.J., Li, G.H., Wang, H., 2021. Efficient removal of arsenic from copper smelting wastewater via a synergy of steel-making slag and KMnO4. In: Li, Y.K., Qi, X.J., Li, G. H., Wang, H. (Eds.), JOURNAL OF CLEANER PRODUCTION, 287.
Li, Zhang, Y., Wang, F.H., Wang, L., Liu, J., Hashimoto, Y., Hosomi, M., 2021. Arsenic immobilization and removal in contaminated soil using zero-valent iron or magnetic biochar amendment followed by dry magnetic separation. In: Li, J.N., Zhang, Y., Wang, F.H., Wang, L., Liu, J., Hashimoto, Y., Hosomi, M. (Eds.), SCIENCE OF THE TOTAL ENVIRONMENT, 768.
Li, Y.K., Zhu, X., Qi, X.J., Shu, B., Zhang, X., Li, K.Z., Wang, H., 2020. Efficient removal of arsenic from copper smelting wastewater in form of scorodite using copper slag. Article 122428 J. Clean. Prod. 270. https://doi.org/10.1016/j.jclepro.2020.122428.
Lian, F., Liu, X.W., Gao, M.L., Li, H.Z., Qiu, W.W., Song, Z.G., 2020. Effects of Fe-Mn-Ce oxide-modified biochar on As accumulation, morphology, and quality of rice (Oryza sativa L.). Environ. Sci. Pollut. Res. 27 (15), 18196–18207. https://doi.org/10.1007/s11356-020-08355-6.
Lin, Song, Z., Huang, Y., Khan, Z.H., Qiu, W., 2019. Removal and Oxidation of Arsenic from Aqueous Solution by Biochar Impregnated with Fe-Mn Oxides. In: Lin, L., Song, Z., Huang, Y., Khan, Z.H., Qiu, W. (Eds.), WATER, AIR, & SOIL POLLUTION, 230.
Liu, Gao, M.L., Qiu, W.W., Khan, Z.H., Liu, N.B., Lin, L.N., Song, Z.G., 2019. Fe-Mn-Ce oxide-modified biochar composites as efficient adsorbents for removing As(III) from water: adsorption performance and mechanisms. In: Liu, X.W., Gao, M.L., Qiu, W.W., Khan, Z.H., Liu, N.B., Lin, L.N., Song, Z.G. (Eds.), ENVIRONMENTAL SCIENCE AND POLLUTION RESEARCH, 26, pp. 17373–17382.
Liu, C.L., Guo, W.T., Sun, Z.L., Liu, X.J., Liu, F., Zhao, Z.W., 2024. Study on the properties of anorthite-based porous sound-absorbing materials prepared by steel slag and fly ash. Article 129776 Mater. Chem. Phys. 326. https://doi.org/10.1016/j.matchemphys.2024.129776.
Liu, K., Li, F.B., Cui, J.H., Yang, S.Y., Fang, L.P., 2020. Simultaneous removal of Cd(II) and As(III) by graphene-like biochar-supported zero-valent iron from irrigation waters under aerobic conditions: Synergistic effects and mechanisms. Article 122623 J. Hazard. Mater. 395. https://doi.org/10.1016/j.jhazmat.2020.122623.
Liu, Meng, J., Huang, Y.L., Dai, Z.M., Tang, C.X., Xu, J.M., 2020. Effects of carbide slag, lodestone and biochar on the immobilization, plant uptake and translocation of As and Cd in a contaminated paddy soil. In: Liu, G.F., Meng, J., Huang, Y.L., Dai, Z.M., Tang, C.X., Xu, J.M. (Eds.), ENVIRONMENTAL POLLUTION, 266.
Liu, C.Y., Tian, H.X., Li, H.Y., Xie, W., Wang, Z.Q., Megharaj, M., He, W.X., 2019b. The accuracy in the assessment of arsenic toxicity using soil alkaline phosphatase depends on soil water contents. Ecol. INDICATORS 102, 457–465. https://doi.org/10.1016/j.ecolind.2019.02.061.
Liu, C.P., Yu, H.Y., Liu, C.S., Lie, F.B., Xu, X.H., Wang, Q., 2015. Arsenic availability in rice from a mining area: Is amorphous iron oxide-bound arsenic a source or sink? Environ. Pollut. 199, 95–101. https://doi.org/10.1016/j.envpol.2015.01.025.
Liyun, Y., Mengdan, G., Yan, L., Shaojie, L., Libing, Y., Shuwu, L., 2022. Removal Arsenic (V) Efficiency and Characteristics Using Modified Basic Oxygen Furnace Slag in Aqueous Solution. J. Resour. Ecol. 13 (3). https://doi.org/10.5814/j.issn.1674-764x.2022.03.018.
Loginow, W., Wisniewski, W., Gonet, S.S., Ciescinska, B., 1987. Fractionation of organic carbon based on susceptibility to oxidation. POLISH JOURNAL SOIL SCIENCE (POLAND) 20 (1), 47–52.
Luo, K.L., Zhang, S.X., Tian, Y., Gao, X., 2014. Arsenic distribution pattern in different sources of drinking water and their geological background in Guanzhong Basin, Shaanxi, China. ACTA Geologica Sin.Engl. Ed. 88 (3), 984–994. https://doi.org/10.1111/1755-6724.12251.
Nabi, A., Naeem, M., Aftab, T., Masroor, M., Khan, A., 2019. Arsenic toxicity induced changes in growth, photosynthetic pigments, antioxidant machinery, essential oil, menthol and other active constituents of menthol mint (Mentha arvensis L.).

J. Essent. Oil Bear. Plants 22 (5), 1333–1348. https://doi.org/10.1080/0972060X.2019.1699865.
Ning, X., He, L., Long, S., Wang, S., 2025. Bioavailability, migration and driving factors of As, Cd and Pb in calcareous soil amended with organic fertilizer and manganese oxidizing bacteria in arid northwest China. J. Hazard. Mater. 489. https://doi.org/10.1016/j.jhazmat.2025.137528.
Ning, D.F., Liang, Y.C., Song, A., Duan, A.W., Liu, Z.D., 2016. In situ stabilization of heavy metals in multiple-metal contaminated paddy soil using different steel slag-based silicon fertilizer. Environ. Sci. Pollut. Res. 23 (23), 23638–23647. https://doi.org/10.1007/s11356-016-7588-y.
Oladele, S.O., 2019. Effect of biochar amendment on soil enzymatic activities, carboxylate secretions and upland rice performance in a sandy clay loam Alfisol of Southwest Nigeria. Sci. Afr. 4, e00107. https://doi.org/10.1016/j.sciaf.2019.e00107.
Pawar, R.R., Lalhmunsiama, Kim, M., Kim, J.G., Hong, S.M., Sawant, S.Y., Lee, S.M., 2018. Efficient removal of hazardous lead, cadmium, and arsenic from aqueous environment by iron oxide modified clay-activated carbon composite beads. Appl. Clay Sci. 162, 339–350. https://doi.org/10.1016/j.clay.2018.06.014.
Pérez-Sirvent, C., Hernández-Pérez, C., Martínez-Sánchez, M.J., García-Lorenzo, M.L., Bech, J., 2016. Geochemical characterisation of surface waters, topsoils and efflorescences in a historic metal-mining area in Spain. J. Soils Sediment. 16 (4), 1238–1252. https://doi.org/10.1007/s11368-015-1141-3.
Prayogo, C., Jones, J.E., Baeyens, J., Bending, G.D., 2014. Impact of biochar on mineralisation of C and N from soil and willow litter and its relationship with microbial community biomass and structure. Biol. Fertil. Soils 50 (4), 695–702. https://doi.org/10.1007/s00374-013-0884-5.
Qiao, J.T., Liu, T.X., Wang, X.Q., Li, F.B., Lv, Y.H., Cui, J.H., Liu, C.P., 2018. Simultaneous alleviation of cadmium and arsenic accumulation in rice by applying zero-valent iron and biochar to contaminated paddy soils. Chemosphere 195, 260–271. https://doi.org/10.1016/j.chemosphere.2017.12.081.
Seyfferth, A.L., Amaral, D., Limmer, M.A., Guilherme, L.R.G., 2019. Combined impacts of Si-rich rice residues and flooding extent on grain As and Cd in rice. Environ. Int. 128, 301–309. https://doi.org/10.1016/j.envint.2019.04.060.
Shao, N.N., Li, S., Yan, F., Su, Y.P., Liu, F., Zhang, Z.T., 2020. An all-in-one strategy for the adsorption of heavy metal ions and photodegradation of organic pollutants using steel slag-derived calcium silicate hydrate. Article 121120 J. Hazard. Mater. 382. https://doi.org/10.1016/j.jhazmat.2019.121120.
Shi, W., Li, H., Liao, G., Pei, G., Lin, Y., 2018. Carbon steel slag and stainless steel slag for removal of arsenic from stimulant and real groundwater. Int. J. Environ. Sci. Technol. 15 (11), 2337–2348. https://doi.org/10.1007/s13762-017-1603-9.
Tan, S.M., Narayanan, M., Huong, D.T.T., Ito, N., Unpaprom, Y., Pugazhendhi, A., Liu, J. A., 2022. A perspective on the interaction between biochar and soil microbes: a way to regain soil eminence. Article 113832 Environ. Res. 214. https://doi.org/10.1016/j.envres.2022.113832.
Tian, F., Wang, Y.W., Zhao, Y.W., Sun, R.Y., Qi, M., Wu, S.Q., Wang, L., 2025. A review of biochar-industrial waste composites for sustainable soil amendment: mechanisms and perspectives. Article 2184 Water 17 (15). https://doi.org/10.3390/w17152184.
Uchimiya, M., Ohno, T., He, Z.Q., 2013. Pyrolysis temperature-dependent release of dissolved organic carbon from plant, manure, and biorefinery wastes. J. Anal. Appl. Pyrolysis 104, 84–94. https://doi.org/10.1016/j.jaap.2013.09.003.
Van Zwieten, L., Kimber, S., Morris, S., Chan, K.Y., Downie, A., Rust, J., Cowie, A., 2010. Effects of biochar from slow pyrolysis of papermill waste on agronomic performance and soil fertility. Plant Soil 327 (1-2), 235–246. https://doi.org/10.1007/s11104-009-0050-x.
Wan, X.M., Li, C.Y., Parikh, S.J., 2020. Simultaneous removal of arsenic, cadmium, and lead from soil by iron-modified magnetic biochar. Article 114157 Environ. Pollut. 261. https://doi.org/10.1016/j.envpol.2020.114157.
Wang, S.S., Gao, B., Zimmerman, A.R., Li, Y.C., Ma, L., Harris, W.G., Migliaccio, K.W., 2015. Removal of arsenic by magnetic biochar prepared from pinewood and natural hematite. Bioresour. Technol. 175, 391–395. https://doi.org/10.1016/j.biortech.2014.10.104.
Wang, S.S., Li, W.J., Ding, C.Y., Zhang, J., Zhang, N., Li, Y.C.C., Wang, X.Z., 2024. Biochar-supported zero-valent iron enhanced arsenic immobilization in a paddy soil: the role of soil organic matter. Article 26 Biochar 6 (1). https://doi.org/10.1007/s42773-024-00318-1.
Wang, Y.H., Morin, G., Ona-Nguema, G., Brown, G.E., 2014. Arsenic(III) and Arsenic(V) speciation during transformation of lepidocrocite to magnetite. Environ. Sci. Technol. 48 (24), 14282–14290. https://doi.org/10.1021/es5033629.
Wang, F., Tong, Y.A., Zhang, J.S., Gao, P.C., Coffie, J.N., 2013. Effects of various organic materials on soil aggregate stability and soil microbiological properties on the Loess Plateau of China. Plant Soil Environ. 59 (4), 162–168. https://doi.org/10.17221/702/2012-PSE.
Wei, M., Wang, B., Chen, M., Wu, P., Zhang, X., 2025. Remediation of antimony and arsenic in co-contaminated soil by electrolytic manganese residue-biochar composite: effects, mechanisms, and microbial response. Environ. Pollut. 366. https://doi.org/10.1016/j.envpol.2024.125371.
Wei, M., Wang, B., Wu, P., Zhang, X.Y., Chen, M., Wang, S.S., 2024. Electrolytic manganese residue-biochar composite for simultaneous removal of antimony and arsenic from water: adsorption performance and mechanisms. Article 140623 J. Clean. Prod. 437. https://doi.org/10.1016/j.jclepro.2024.140623.
Yamada, A., Mohri, S., Nakamura, M., Naruse, K., 2010. A fully automated pH measurement system for 96-well microplates using a semiconductor-based pH sensor. Sens Actuators B Chem. 143, 464–469.
Yang, X., Fan, J., Jiang, L., Zhu, F., Yan, Z., Li, X., Xue, S., 2024. Using Fe/H2O2-modified biochar to realize field-scale Sb/As stabilization and soil structure improvement in an Sb smelting site. Sci. Total Environ. 912. https://doi.org/10.1016/j.scitotenv.2023.168775.
Yang, D., Yang, S.Y., Wang, L., Xu, J.M., Liu, X.M., 2021. Performance of biochar-supported nanoscale zero-valent iron for cadmium and arsenic co-contaminated soil remediation: insights on availability, bioaccumulation and health risk. Article 118054 Environ. Pollut. 290. https://doi.org/10.1016/j.envpol.2021.118054.
Yuan, C.G., He, B., Gao, E.L., Lü, J.X., Jiang, G.B., 2007. Evaluation of extraction methods for arsenic speciation in polluted soil and rotten ore by HPLC-HG-AFS analysis. Microchimica ACTA 159 (1-2), 175–182. https://doi.org/10.1007/s00604-006-0709-4.
Zaw, A.C.C., Gathuka, L.W., Takai, A., Katsumi, T., 2022. Effects of adding slags on strength and leaching properties of soft soil. J. Mater. Cycles Waste Manag. 24 (4), 1423–1431. https://doi.org/10.1007/s10163-022-01442-5.
Zhang, M., Cheng, G., Feng, H., Sun, B.H., Zhao, Y., Chen, H.X., Zhang, A.F., 2017. Effects of straw and biochar amendments on aggregate stability, soil organic carbon, and enzyme activities in the Loess Plateau, China. Environ. Sci. Pollut. Res. 24 (11), 10108–10120. https://doi.org/10.1007/s11356-017-8505-8.
Zhang, Y.L., Hou, Z.W., Fu, P.F., Wang, X.F., Xue, T.L., Chen, Y.Q., 2023. Remediation of As-contaminated soil by utilizing steel slag-based passivators with different Fe/Ca ratios: as bioavailability and passivation characterization. Article 139219 J. Clean. Prod. 427. https://doi.org/10.1016/j.jclepro.2023.139219.
Zhang, Z., Zheng, X., Li, J., Xu, G., Tan, L., 2024. Mechanism of reinforced interfacial adhesion between steel slag and highly devulcanized waste rubber modified asphalt and its influence on the volume stability in steel slag asphalt mixture. Constr. Build. Mater. 447, 138129. https://doi.org/10.1016/j.conbuildmat.2024.138129.
Zheng, L.D., Zhang, M.X., Xiao, R., Chen, J.X., Yu, F.H., 2017. Impact of salinity and Pb on enzyme activities of a saline soil from the Yellow River delta: a microcosm study. Phys. Chem. EARTH 97, 77–87. https://doi.org/10.1016/j.pce.2016.11.001.